Atmospheric
Chemistry
and Physics
Discussions

Open Access

Mesoscale modeling of smoke transport over the Southeast Asian Maritime Continent: coupling of smoke direct radiative feedbacks below and above the low-level clouds

C. Ge[1,2], J. Wang[1], and J. S. Reid[3]

[1]Department of Earth and Atmospheric Sciences, University of Nebraska – Lincoln, NE, USA
[2]State Key Laboratory of Atmospheric Boundary Layer Physics and Atmospheric Chemistry, Institute of Atmospheric Physics, Chinese Academy of Sciences, Beijing, China
[3]Naval Research Laboratory, Monterey, CA, USA

Correspondence to: J. Wang (jwang7@unl.edu)

ACPD

13, 15443–15492, 2013

Mesoscale modeling of smoke transport

C. Ge et al.

Title Page

Abstract	Introduction
Conclusions	References
Tables	Figures

Back | Close

Full Screen / Esc

Printer-friendly Version

Interactive Discussion

Abstract

The online-coupled Weather Research and Forecasting model with Chemistry (WRF-Chem) is used to simulate the direct and semi-direct radiative impacts of smoke particles over the Southeast Asian Marine Continents (MC, $10° S–10° N$, $90° E–150° E$) during October 2006 when a significant El Nino event caused the highest biomass burning activity since 1997. With the use of OC (Organic Carbon)/BC (Black Carbon) ratio of 10 in the smoke emission inventory, the baseline simulation shows that the low-level clouds amplifying effect on smoke absorption led to a warming effect at the top-of-atmosphere (TOA) with a domain/monthly average forcing value of $\sim 20\,\mathrm{W\,m^{-2}}$ over the islands of Borneo and Sumatra. The smoke-induced monthly average daytime heating ($0.3\,\mathrm{K}$) that is largely confined above the low-level clouds results in the local convergence over the smoke source region. This heating-induced convergence coupled with daytime planetary boundary layer turbulent mixing, transports more smoke particles above the planetary boundary layer height (PBLH), hence rendering a positive feedback. This positive feedback contrasts with the decrease of cloud fraction resulted from the combined effects of smoke heating within the cloud layer and the more stability in the boundary layer; the latter can be considered as a negative feedback in which decrease of cloud fraction weakens the heating by smoke particles above the clouds. During nighttime, the elevated smoke layer (above clouds in daytime) is decoupled from boundary layer, and the reduction of PBLH due to the residual surface cooling from the daytime lead to the accumulation of smoke particles near the surface. Because of smoke radiative extinction, on monthly basis, the amount of the solar input at the surface is reduced as large as $60\,\mathrm{W\,m^{-2}}$, which lead to the decrease of sensible heat, latent heat, 2 m air temperature, and PBLH by a maximum of $20\,\mathrm{W\,m^{-2}}$, $20\,\mathrm{W\,m^{-2}}$, $1\,\mathrm{K}$, $120\,\mathrm{m}$, respectively. The decrease of boundary layer mixing and the generation of convergence above the PBL also results in a reduction of precipitable water 1–2 km above the PBLH and more precipitable water near the surface and in upper part of the middle troposphere with changes around $0.1\,\mathrm{mm}$. Overall, there is

less of a change of column water vapor over the land, and an increase of water vapor amount over the Karimata Strait. The cloud changes over continents are mostly occurred over the islands of Sumatra and Borneo during the daytime, where the low-level cloud fraction decreases more than 10 %. However, the change of local wind (include sea breeze) induced by the smoke radiative feedback leads to more convergence over Karimata Strait and south coastal area of Kalimantan during both daytime and night time; consequently, cloud fraction is increased there up to 20 %. The sensitivities with different OC/BC ratio show the importance of the smoke single scattering albedo for the smoke semi-direct effects. A case study on 31 October 2006 further demonstrated a much larger (more than twice of the monthly average) feedback induced by smoke aerosols. The decreased sea breeze during big events can lead to prominent increase (40 %) of low-level cloud over coastal water. Lastly, the direct and semi-direct radiative impact of smoke particles over the Southeast Asian Marine Continents is summarized as a conceptual model.

1   Introduction

In September and October 2006, moderate El Nino conditions resulted in negative precipitation anomolies in the Southeast Asian Maritime Continent (MC, 10° S–10° N, 90° E–150° E). Subsequent drought conditions then led to the most significant biomass burning activity since the massive 1997 event which first drew attention to the region (van der Werf et al., 2008; Reid et al., 2012). For the first time, a large El Nino induced burning season could be observed by the NASA's Afternoon or A-train satellite constellation and characterized models with advanced data assimilation. In total, ~ 3.5 Tg smoke particles were emitted according to the Fire Locating and Modeling of Burning Emissions (FLAMBE) estimate (Reid et al., 2009; Wang et al., 2013). Fires in Sumatra and Borneo contributed to 24 h mean PM_{10} concentrations above $150\,mg\,m^{-3}$ at multiple locations in Singapore and Malaysia over several days (Hyer and Chew, 2010; Wang et al., 2013).

This study investigates the radiative effect of smoke particles on planetary boundary layer properties during October 2006 in the MC, when regional smoke concentrations and AODs were at a regional maximum for the last decade (Reid et al., 2012; Wang et al., 2013; Xian et al., 2013). Indeed, MODIS average clear sky mid-visible AODs were over 0.8 for a large band stretching from Sumatra through Borneo for this period (Xian et al., 2013). A study of this period would then provide an upper end benchmark on aerosol-boundary layer meteorology feedbacks in the region. Indeed, the significance of the smoke radiative effect over the Asian MC has also been recognized by several past studies, but mainly from both satellite data and global chemistry models (e.g., Duncan, 2003; Podgorny et al., 2003; Davison et al., 2004; Parameswaran et al., 2004; Rajeev, 2004; Thampi et al., 2009; Ott et al., 2010). Based on a radiative transfer model, Podgorny et al. (2003) studied aerosol radiative forcing of 1997 Indonesia forest fire and showed that the low level clouds embedded in the absorbing aerosols increase aerosol-induced absorption in the troposphere, and decrease the magnitude of aerosol forcing at the TOA (also see Podgorny and Ramanathan, 2001). They concluded that relatively small changes in low-level cloud fraction and single scattering albedo (SSA) might result in significant changes in the magnitude and even the sign of the TOA forcing. As discussed in Reid et al. (2012, 2013) and Wang et al. (2013), the distribution of smoke particles over the MC is affected by an interplay of meteorological systems at various temporal and spatial scales, including the ENSO, ITCZ/monsoon and trade winds at larger scales, the MJO and typhoons at mesoscale, and the sea breezes, topography and boundary layer process at local scales. Different from previous analyses, our focus here is to investigate how the smoke direct radiative effects are regulated by and feedback to the meteorology at regional to local scales. This study is the second part of a series of our mesoscale modeling efforts for the 7 Southeast Asian Studies (7SEAS) project (among many other research goals) to reveal the production, transport and radiative effects of aerosols in MC (Campbell et al., 2012; Feng and Christoipher, 2012; Hyer et al., 2013; Reid et al., 2012, 2013; Salinas et al., 2013; Wang et al., 2013; Xian et al., 2013). Here, we examine the radiative impacts of smoke particles

from mesoscale simulations of Wang et al. (2013) in which an online-coupled regional Weather Research and Forecasting model with Chemistry (WRF-Chem) was used in conjunction with satellite data from MODIS and CALIOP and ground-based $PM_{2.5}$ data to identify the smoke transport pathway under the influence of aforementioned multi-scale meteorological factors.

It is well known that the direct radiative effect of smoke particles and the radiative feedback on meteorology highly depends on the smoke single scattering albedo, smoke amount or smoke aerosol optical depth (AOD), not only in column but also in different vertical layers (Wang and Christopher, 2006, and references therein). Specific to the MC smoke particles, their single scattering properties have not been well studied (Davison, 2004; Reid et al., 2013), although past analysis (such as Tosca et al., 2011; Campbell et al., 2013; Wang et al., 2013, and references therein) have shown that smoke particles are primarily located within or just above the boundary layer (~ 1.5–2 km above the surface). Our current study is designed to conduct a series of numerical experiments with perturbations in particle single scattering characteristics, and evaluate how smoke's radiative effects can influence and feedback with boundary layer properties, such as air temperature, sensible and latent heat fluxes, boundary layer height and cloud cover in a complex meteorological environment such as in MC. The goal of the paper is to relate possible physical mechanisms at regional-to-local scale, rather than to quantify exactly the impact of smoke radiative effect; the latter certainly won't be likely until the aerosol optical properties are well characterized in the conclusion of the 7SEAS field campaign.

The numerical experiments presented here are based upon Wang et al. (2013) that showed, when FLAMBE smoke emissions should be doubled and be injected within 800 m above surface, a good agreement can be found between simulation from WRF-chem and satellite/ground-based observations in terms of surface $PM_{2.5}$ mass, aerosol vertical profile, and smoke transport path. However, while similar model configuration (as in Wang et al., 2013) will be used for the numerical experiments in this study, this study differ from Wang et al. (2013) in that smoke direct radative effect and feedback

(e.g., semi-direct effect) are studied, and the impact of uncertainty in smoke single scattering albedo is investigated. Generally, besides the direct effects (scattering and absorbing incoming solar radiation), aerosols can indirectly influence the climate by acting as cloud condensation nuclei (CCN) and/or ice nuclei (CN), and thereby modifying the microphysics, radiative properties and life time of clouds. Several studies (e.g. Reid et al., 1998; Feingold et al., 2001; Koren et al., 2008) implies indirect effects are most evident under clean conditions with less number of background aerosols, but in heavily polluted background, the aerosol indirect effect can be saturated or indiscernible. Since during our study period $PM_{2.5}$ concentration is always high over MC (Wang et al., 2013), although the aerosols indirect effect is very important, it's perturbation due to the aerosol at such high particle concentration condition could be not as sensible as direct effect, especially over smoke source regions. The indirect effects might become critically prominent over the area further out from the MC and therefore are planned for our future study.

While the single scattering albedo of smoke particles is known to be highly dependent on its relative composition of black carbon and organic mass (Reid et al., 2005), the dearth of in situ measurements for characterizing the smoke properties in MC make it impossible for us to find an optimal BC/OC ratio for use in WRFChem (Reid et al., 2013). Instead, we conduct the WRFChem simulation for a set of BC/OC ratios, and analyze the sensitivity of smoke direct radiative forcing and its associated radiative feedback on atmosphere to the OC/BC ratio used in the smoke emission. We describe the experiment design (including the WRF-chem model and data used in this study) in Sect. 2, and present the baseline modeled results of the smoke radiative impact on surface energy budget and the associated feedbacks on dynamics and the distribution of various meteorological fields in Sect. 3. In Sect. 4, we conduct model sensitivity simulations to ascertain the impact of the smoke with different OC/BC ratio, and in Sect. 5 we provide a detailed analysis of the seasons most significant events. A conceptual model that illustrates the finding of this study is given in Sect. 6, while itemized summaries are provided in Sect. 7.

2 Model description

2.1 Configuration of WRF-chem

The WRF-chem model (Fast et al., 2006; Grell et al., 2005) can be used for weather forecast and regional climate studies as well as be used to simulate gas phase chemistry, aerosol life cycle, and aerosol-cloud-radiation interactions. The model configuration in this study is similar as the one in Wang et al. (2013), and Table 1 lists the model configuration options employed in this study.

According to the database compiled by Barnard et al. (2010), the refractive index of BC in this study is assigned the value of $1.85 + i0.71$ for 550 nm, and the value for OC (dry) is 1.45 for 300 nm to 800 nm. The density of BC and OC is assumed to be $1.7\,\mathrm{g\,cm^{-3}}$ and $1\,\mathrm{g\,cm^{-3}}$, respectively. The hydroscopicity is assumed to be 0.14 for OC and a very small nonzero value (10^{-6}) for BC (Ghan et al., 2001a). Refractive indices and optical properties are computed with Mie parameterizations that are function of wet surface mode radius and refractive indices of wet aerosol in each mode (Zhang, Y., 2008). The size distributions of OC and BC emissions are both represented as accumulation mode with volume mean diameter of 0.3 μm and standard deviation of 2.

It is worth noting that only smoke particle emission (portioned as BC and OC) is considered in the current WRF-chem simulation. As shown in Wang et al. (2013), smoke emission overwhelm dominates other emissions in September–October 2006, and to be consistent with our interest of smoke radiative effect and to avoid large uncertainties in the simulation of secondary organic aerosols, the emission from other sources including industrial emission, biogenic emission, and wind-blow sea salt are not implemented in the simulation. Our experiment design here follows the strategy of Wang and Christpher (2006) in which they studied the radiative impact of Central American smoke particles by considering the particle emission only. Similar as Wang et al. (2013), smoke emission inventory from FLAMBE is used to specify the source of BC and OC (with different BC and OC emission ratios as described in the following section) as a function of time (with an updates of every 6 h). In the model, the injec-

tion height of smoke (OC and BC) emissions is specified as 800 m above the surface (Wang, 2013).

The 1°×1° National Center for Environmental Prediction (NCEP) Final Analysis (FNL) data at 00:00, 06:00, 12:00 and 18:00 UTC are used for initializing and specifying the temporally evolving lateral boundary conditions. The time-varying sea surface temperature (SST), sea ice, vegetation fraction, and albedo were updated every 6 h from the NCEP reanalysis data during the model simulation. We notice that the use of 6 h nudged SST may not ideal for studying the response of SST to the feedback of smoke aerosol. However, this non-ideality has to be compromised because of the luck of a fully coupled ocean model within WRFChem. Furthermore, as shown in Wang et al. (2013), most smoke particles are indeed over the land and over the ocean close to the maritime continents, and so a large scale change of SST due to smoke radiative effects is unlikely. In addition, the temperature contrast between coastal ocean and land is well demonstrated by the simulated change of sea breeze (Wang et al., 2013), which also partly supports that the use of nudged SST, while not ideal, is practically reasonable for this study to analyze smoke radiative effect and feedback.

2.2 Experiment design

The relative mass fraction of BC and OC in smoke particles can vary significantly, depending on the composition of the biomass burned, the fire temperature (that regulates the phases of flaming and smoldering in the combustion), and the particle age (Andreae and Merlet, 2001; Kleeman et al., 2000; Liousse et al., 1995; Reid et al., 2005b, 2012, 2013). The review by Reid et al. (2005a) showed BC typically accounts for 4–8 % smoke particle dry mass and approximately 50–65 % of mass is attributable to organic carbon. To date, analysis of BC/OC ratio for smoke particles in Maritime Continent (MC) has been limited (Akagi et al., 2011; Kondo et al., 2011; Page et al., 2002; Sahu et al., 2011; See et al., 2006) and deserves a special attention because burning of peatland (to transform it into farmland) is a main contributor to smoke aerosol emission in MC

during El Nino years, albeit that agricultural and lowland forest burning and wildfires in rainforest vegetation may also contribute, particularly in neutral or wet years.

In this study, three different ratios of OC/BC as 3.5, 10 and 17 respectively are selected and used in WRFChem. In doing so, we can obtain a wider range in model climate response that offer a perspective on the radiative impacts of BC aerosols over Southeast Asia Maritime Continent. Four sets of simulations are performed in this study and the detail can be seen as Table 2. In all simulations, the total amount of emitted particulate organic matter (1.5 × OC mass) and BC amount are kept the same, which is 90 % of the total smoke particle mass (that is estimated in FLAMBE, and consistent with Herner et al., 2005; Lim and Turpin 2002; Matthew and Kimberly, 2006). All numerical simulations are initiated at 00:00 UTC on 20 September 2006 and ended at 00:00 UTC on 2 November 2006. However, only data during 1 October–31 October 2006 are analyzed, during which the most smoke events occurred (Wang et al., 2013). Except in Sect. 5, all variables in the analysis are monthly averaged over October 2006.

3 Baseline results (OC/BC = 10)

3.1 Smoke radiative impact at surface and TOA

Monthly average aerosol, radiation, and cloud features for October 2006 are presented in Fig. 1. This corresponds to a post monsoonal shift and regional drying event that leads to the largest El Nino based fire events in the region (Reid et al., 2012). Discussion of regional meteorology for this specific period can be found in Wang et al. (2013). Two regions with high aerosol optical depth (AOD) and high absorption aerosol optical depth (AAOD) values are found in the monthly mean (full sky conditions) of model simulations (Fig. 1a); they are respectively located at the Kalimantan region and the Sumatra region, the two areas of large fire emissions (Wang et al., 2013) and relatively low topography (Fig. 1c). All-sky AOD average here is 30–50 % lower than that from MODIS AOD retrievals (as showed in Xian et al., 2013), in part reflecting the

Title Page

Abstract | Introduction

Conclusions | References

Tables | Figures

◄ | ►

◄ | ►

Back | Close

Full Screen / Esc

Printer-friendly Version

Interactive Discussion

40 % difference between clear-sky and all-sky AODs (Zhang and Reid, 2009). Higher TOA shortwave direct radiative forcing (SWDRF) induced by smoke aerosol particles mainly occur over areas aforementioned associated with high smoke AOD (Fig. 1e), and deferent with usual case, positive SWDRF ($\sim 15\,\mathrm{W\,m^{-2}}$) takes place.

There is higher contrast (and spatial discontinuity) in SWDRF between land and ocean than that of AOD. Larger values are not only over the land in high emissions area, but also over the Indian Ocean close to the southwest of Sumatra (Fig. 1e). The positive forcing at the TOA can be understood through two factors: (a) the single scattering albedo of smoke particles, which is about 0.9 (based upon AOD and AAOD distribution shown in Fig. 1) and governs the portion of solar energy that are lost in the atmosphere due to absorption by the smoke particles; (b) the underlying surface or cloud properties (for aerosol layer) that regulates the amount of solar energy being re-direct (through reflection or multi-scattering) for the smoke particles to absorb/reflect (Hansen et al., 1997). Detailed analysis show that (b) is a dominate factor in our study region because: (i) in October boundary clouds are generally persistent throughout the region, particular in the west Sumatran Low (Reid et al., 2012, 2013), (ii) neither the distribution of AOD (with high spatial variation from 0.1 to 1.1, Fig. 1a) nor absorption aerosol optical depth (AAOD with small spatial variation from 0.17 to 0.20, Fig. 1b) over the 8° S–0° zone reflect the land/ocean discontinuity of SWDRF; (iii) large positive SWDRF are in the locations where outgoing shortwave flux (O-SW) at the TOA is also high (Fig. 1d) due to large cloud fraction, (iv) the discontinuity (e.g., less than $60\,\mathrm{W\,m^{-2}}$) of outgoing shortwave at TOA between the land and sea reflects the impact of sea breeze (Wang et al., 2013) and the resultant low cloud fraction during daytime along the coast.

The transport analysis of vertical profile of smoke and cloud over the source region of smoke of this month in Wang et al. (2013) showed that significant amount of smoke particles are within and above the low-level cloud layer (also, later see discussion of Fig. 6a, c and f). To further confirm that the warming at the TOA is due to aerosol particles above and mixing with the cloud, we also analyze the SWDRF in clear sky

conditions (with cloud fraction less than 0.05, Fig. 1f) and find the strong negative forcing (up to $-20\,\mathrm{W\,m^{-2}}$). This also partially explains some of the negative forcing in full-sky conditions such as in the area around Borneo island with less cloud fraction. By restricting the analysis of SWDRF at TOA in conditions of cloud fraction less than

5 0.05 respectively for low-level cloud, mid-level cloud, and high-level cloud only (Fig. 1 g–i), we found that SWDRF in low-level cloud fraction of less than 0.05 (Fig. 1g) is very similar to that of in conditions with all cloud fraction less than 0.05 (Fig. 1f) while SWDRFs both for middle-level and high-level cloud fraction less than 0.05 are similar to that in all sky conditions, all of which suggests that the low-level cloud plays more

10 important role than mid-level and high-level clouds to cause the positive forcing of smoke aerosols.

    As a result of extinction of solar radiative flux by smoke particles in the atmosphere, the net short wave flux at surface or ground (GSW) is reduced (Fig. 1k). Large reductions are in regions where cloud fraction (as indicated by the outgoing shortwave

15 at TOA, Fig. 1d) is low and AOD (Fig. 1a) is relatively high. As large as $60\,\mathrm{W\,m^{-2}}$ of GSW is reduced in the Kalimantan region and the nearest area of Karimata strait to Kalimantan, and $\sim 30\,\mathrm{W\,m^{-2}}$ of reduction in the downwind ocean region, which respectively corresponding to $\sim 20\,\%$ and $10\,\%$ of the net solar input or GSW at the surface (Fig. 1j). It is interesting to note that distribution of GSW (Fig. 1j) exhibits generally

20 opposite pattern as that of outgoing shortwave at TOA (Fig. 1d), showing larger values (an increase of $\sim 100\,\mathrm{W\,m^{-2}}$compared to that over land) along the coast ocean due to the small cloud fraction (induced by sea breeze). Analysis of the change of GSW (ΔGSW) by smoke particles in clear sky conditions (with cloud fraction less than 0.05, Fig. 1l) shows much larger reduction of GSW than the counterparts in full sky con-

25 dition, especially over the smoke source region; this difference again underscore the importance of relative vertical position between aerosols and clouds in the estimate of full sky aerosol radiative effect.

    With a climate model at a spatial resolution of 3.75° longitude by 2.5° latitude, Davison et al. (2004) estimated the smoke radiative forcing at surface as a result of the In-

Mesoscale modeling of smoke transport

C. Ge et al.

Title Page

Abstract	Introduction
Conclusions	References
Tables	Figures

⏮   ⏭

◀   ▶

Back   Close

Full Screen / Esc

Printer-friendly Version

Interactive Discussion

donesia forest fires in September 1997 is $\sim 200\,\mathrm{W\,m^{-2}}$ or a 75 % reduction of the total incident SW flux. The difference between our estimate and that in Davison et al. (2004) may in part due to the different in smoke emission; the smoke emission in September–October 2006 is estimated as $\sim 3.48\,\mathrm{Tg}$ after the doubling of FLAMBE's emission (Wang et al., 2013) and thus is much lower than $26.07\,\mathrm{Tg}$ for the same two months in 1997 (Davison et al., 2004), although both estimates bear uncertainty by a factor of 2 (Reid et al., 2013).

Further detailed contrast of Fig. 1c with Fig. 1k reveals the impact of topography on the smoke transport and its associated radiative effects. Simulated at spatial resolution of 27 km, the results show very minimal effect of smoke on GSW over the Barisan mountain range along western side of Sumatra Island, and the Tama Abu Mountain that covers half of north Borneo Island. Due to the obstruction of Barisan mountain, the smoke transport path way under southerly trade wind bifurcates into two branches confined respectively at eastern and western side of Barisan mountain, which lead to divergence of smoke concentration and consequently the smaller reduction of GSW over the mountain area. Interestingly, the spatial distributions of simulated outgoing shortwave (Fig. 1d) and GSW distribution (Fig. 1j) both reflect the influence of topography and land use change. Regions with high (low) elevation generally have low (high) surface albedo and hence larger (lower) GSW and smaller (larger) outgoing shortwave. Such fine-scale topography-related features of the radiative transfer calculation are not manifested in the results by Davison et al. (2004) and Ott et al. (2010) from model simulations with coarser resolution, and consequently, the aerosol loading and smoke forcing over the Indian ocean shown in their studies may have an overestimation (as mountain's blocking of smoke transport is not well resolved in the model). Similar kind of overestimation can be also found in Duncan (2003) in which the transport of smoke particles from the 1997 Indonesian wildfires events is simulated with a GEOS-CHEM model at 2.5° longitude by 2° latitude horizontal resolution.

In response to smoke-induced change of radiation at both surface and TOA is the change of surface energy budget and the surface temperature, which is depicted in

Fig. 2. Over the land region both sensible heat (SH, Fig. 2a) and latent heat (LH, Fig. 2c) show a south-north gradients, with highest SH and lowest LH respectively in the south. This pattern of SH is consistent with the spatial distribution of GSW and also 2 m temperature (T2) (Fig. 2e). Generally, less cloud lead to more downward GSW

5 radiation and hence higher T2; higher SH can be found such as the south part of Kalimantan, southeastern Sumatra region, Indonesia and south Sulawesi (Fig. 2a). The pattern of LH more or less reflects the availability of water at the surface and the surface wind speed (Fig. 5e and g), with both having higher values over the ocean (than over land). Due to less availability of soil moisture and precipitation at land area

10 to the south of 2° S (Fig. 3c), LH there is lower compared to the northern land region. The partition of net radiative energy at surface in the form of SH is smaller than that in the form of LH except the land region at south of 2° S, which is consistent with the Bowen ratio (ratio of sensible to latent heat, B) distribution with values of ∼ 0.05 over ocean ∼ 0.5 over land area, ∼ 0.2 for tropical forests and ∼ 1–10 in dry land to deserts

15 (Stull et al., 2000).

As a result of the reduction of GSW, both sensible heat flux at the surface (SH) (Fig. 2b) and latent heat (LH) (Fig. 2d) are decreased up to $20 \, \mathrm{W\,m^{-2}}$ in Kalimantan and Sumatra region. The large reduction of both SH and LH is confined mainly over the land (in particular smoke source) region (Fig. 2b, d), while no evident change of

20 SH and LH can be found over ocean. Similarly, the change of T2 (ΔT2) as a result of the smoke radiative feedback is most significant over land than over open oceans that have a much larger heat capacity and latent heat release (Levitus, S. et al., 2012). Note, since WRF-chem does not have a multi-layer ocean model, simulated here for the ocean are the bulk sea surface temperature (not the sea surface skin temperature).

25 When compared to the land surface temperature, the monthly mean of sea surface temperature generally shows much less variation and are more regulated by the oceanic currents and deep mixing that are not simulated in the WRF-chem. Hence, the changes of SH and LH due to the smoke radiative effect are only restricted over the land areas (as shown in Fig. 2b, d), which is also consistent with Wang and Christopher (2006).

Because of the large reduction of GSW at the surface, T2 decreases by up to 1 K and 0.5 K respectively during day time (between 08:00 LT and 19:00 LT) over the Kalimantan and Sumatra regions that have high loading of smoke aerosols (Fig. 2f). This decrease also has a residual effect at night, leading to a decrease of night temperature by 0.1 K in both regions (Fig. 2h). In contrast, because of the enhanced heating ($\sim$ 2–3 K/day during noon, Fig. 6d) due to the absorption of solar radiation by smoke particles, T at 2200 m above the surface increases by up to 0.6 K and 0.2 K respectively during the daytime in Kalimantan and Sumatra region (Fig. 2j), but this increase has nearly zero residual effect at night (Fig. 2l). It is interesting to note that the model well captures the higher T2 over land (except regions with high topography) and lower T2 over the ocean during daytime (Fig. 2e), and the opposite contrast during nighttime (Fig. 2g). However, neither such day-to-night contrast nor land-to-ocean contrast are seen at 2200 m above the surface, reflecting the low boundary height at this region (Wang et al., 2013), and efficient transport of heat in the atmosphere.

3.2 Smoke radiative feedbacks on boundary layer processes

To a large extent, the distribution of the Planetary Boundary layer Height (PBLH, Fig. 3a) resembles that of T2 (Fig. 2e) and is opposite to that of cloud cover as indicated in outgoing shortwave in Fig. 1d. With less cloud cover and warmer land surface, PBLH in average is higher over the two smoke source regions respectively in south Sumatra and south Kalimantan (Fig. 3a). In response to the decrease of surface temperature and the increase of heating rate in the atmosphere due to smoke absorption, the atmospheric stability is increased in the lower troposphere, and the turbulent mixing process within PBL decreases. This consequently results in a reduction of PBLH up to 120 m (or $\sim$ 10 %) over Sumatra and Kalimantan region in monthly averages (24 h) (Fig. 3b). The distribution of this reduction is similar to the change of T2 (Fig. 2f) with minimal values over the ocean. Although more stability is introduced to the PBL by the smoke aerosol over fire area and most downwind region, over a narrow belt region of Karimata Strait and south coastal ocean of Kalimantan PBL seems unstable (Fig. 3b),

the reason for which will be stated in conjunction with the change of local wind (Fig. 7) in Sect. 3.3.

Figure 3c and d show the distribution of precipitable water and its difference due to smoke radiative impact. Although October is a transition time for ITCZ move southward, in El Nino years winds transit early, leading to broad easterlies across the MC. Reid et al. (2013) suspects an associated inflow of dry tropospheric air from the Australian monsoon suppress convection. From the distribution of precipitable water we can see the distinct line at ∼ 1° S between wet region at north and dry area at south. When considering the feedback of smoke aerosols, increase of precipitable water occurs over fire area and most downwind region, and lager increase occurs over Karimata Strait.

To reveal the dynamical processes that contribute to the change of PBLH as a result of smoke radiative feedback, Fig. 4 show a vertical cross section centered along the latitude of 1° S (5-grid averages) that passes through the densest part of the smoke source region. Included are monthly averages of $PM_{2.5}$ mass concentration, PBLH simulated with (solid line) and without (dotted line) the feedback of smoke radiative aerosols, as well as the differences of temperature (ΔT) and precipitable water (ΔPW). The response of air temperature to the smoke radiative heating in the atmosphere and radiative cooling near the surface depends highly on the aerosol vertical profile that also has an important diurnal variations as a result of boundary layer process (Wang and Christopher, 2006). Because of the dominant subsidence in the upper troposphere over the smoke source region (Fig. 4a; also Wang et al., 2013), the transport of smoke particles to the middle atmosphere is suppressed, and a high concentration of smoke particles can be found around 2–3 km above the boundary layer (Fig. 4a). Note, this smoke layer may be not well characterized by CALIOP because of the co-existence of cloud layer and overlying cirrus clouds (Wang et al., 2013). Nevertheless, this layer is very distinct from the boundary layer during the morning when boundary layer convection has not been well developed (Fig. 4a and red and black lines in Fig. 6a). Correspondingly, during the morning (10:00 LT), an increase of air temperature by up to 0.3 K

can be clearly seen at 1–3 km altitude (Fig. 4c) that is above the boundary layer over the smoke source region.

As time progresses to the late afternoon (17:00 LT) when the convective boundary layer is well developed, the smoke particles are not only well mixed within the boundary layer, but also are transported and mixed with the particles that already exist at 1–3 km from the previous smoke emission (Fig. 4e). Indeed, contrast between Fig. 4a and e shows that the subsidence is much weaker in the middle troposphere ($\sim$ 3–6 km) in the later afternoon as compared to the morning, favorable for the vertical transporting of smoke particle from boundary layer to the middle troposphere. Corresponding increase of air temperature by 0.6 K can be seen over the smoke source region and by $\sim$ 0.1–0.4 K over nearby ocean at altitude of 3–6 km (Fig. 4g). During the night, however, convective boundary layer does not exist, and a residual layer with the decrease of $PM_{2.5}$ between 1 km and 2 km (as a result of changes in the day) is decoupled from the nocturnal boundary layer with an increase of $PM_{2.5}$ (Fig. 4j) that is due to the decrease of boundary layer height. This decoupling is also associated with the shift of upward motion to the downward motion around 1 km in night (Fig. 4i). The temperature change during night is essentially a residual effect from daytime (Fig. 4k).

As discussed in Sect. 3.1, the air temperature change (ΔT) due to smoke particles in the boundary layer is more complex because the warming due to the smoke absorption can be outpaced by the cooling from the surface through turbulent mixing. Indeed, Fig. 4c and g show that cooling occurs nearly everywhere in the boundary layer, but only over the smoke source region, regardless of the time of day. However, in contrast to the mid-altitude warming that is strongest during late afternoon, the cooling is strongest during the morning before more smoke particles are transported to the upper layer to cause warming.

It should be noted that dynamics and radiative effects are coupled; the warming by smoke particles confined over the smoke source region in the morning (10:00 LT) can result in the local convergence and produce the updraft to offset the downdraft above PBLH, which in turn lead to transport more smoke particles above, and thus render

⏮ | ⏭

◀ | ▶

Back | Close

Full Screen / Esc

Printer-friendly Version

Interactive Discussion

a positive feedback. This hypothesis is supported by the following model results: (a) in the morning (10:00 LT) the smoke radiative feedback results in the increase of smoke concentration by $\sim 4\,\mu g\,m^{-3}$ over 2–3.5 km and a similar decrease between 1–2 km, suggesting a local convergence in 1–2 km above the surface; (b) such increase of $PM_{2.5}$ in 2–3.5 km and decrease between 1–2 km are even stronger up to $10\,\mu g\,m^{-3}$ in the later afternoon (17:00 LT), suggesting an enhancement due to the positive feedback.

To illustrate the change of $PM_{2.5}$ introduced by smoke near the surface high emissions areas, we use one of the smoke source regions – Borneo Island as an example (Fig. 5). Borneo Island experienced a distinct rotation of sea breeze and land breeze (Wang et al., 2013). Sea breeze is very strong at 16:00 LT (Fig. 5a), and land breeze is prominent at 00:00 LT (Fig. 5c). When the feedback of aerosols is considered, sea breeze (Fig. 5b) (or land breeze, Fig. 5d) at 16:00 LT (or 00:00 LT) along the south coastal line of Borneo is weakened (or strengthened) up to $0.3\,ms^{-1}$. Hence, convergence (divergence) occurs over south part of Borneo and then the increase (decrease) of smoke aerosols up to $5\,\mu g\,m^{-3}$ can be found at 16:00 LT (00:00 LT). The averaged daytime (or nighttime) change of $PM_{2.5}$ and wind (Fig. 5f and h) show the similar pattern as 16:00 LT (or 00:00 LT). To summarize, the smoke aerosols can cause significant change of the wind circulation at different scale, both vertically and horizontally, and all these changes in turn, can modify the distribution of aerosols.

Unlike the smoke particles that are injected into the atmosphere through fire-produced thermal buoyancy (and considered in the model through the specification of injection height), water vapor is added into the atmosphere from through surface evaporation. However, over the smoke source region where soil is dry compared to the ocean, a large part of the water vapor is from the sea breeze (Fig. 3c). Hence, the response of water vapor amount in boundary layer can differ from that of smoke particles, with former more sensitive to the change of PBLH and turbulent mixing in the PBL, and the latter more sensitive to the change of dynamics around the smoke inject height (of 800 m in this study). Consequently, smoke particle concentrations show nearly no change within PBL, but are decreased near and above the PBLH due to the updraft in

1–2 km where convergence occurs as a result of heating by smoke particles (Fig. 4b and f). In contrast, because of the reduction of PBLH and more stable PBL by the smoke radiative feedback, water vapor is trapped more in the PBL, which in turn leads to less water vapor amount above the PBL in the morning (Fig. 4d). As time progresses toward afternoon, such dichotomy is further amplified, with more water vapor trapped in the PBL and less water vapor above PBL (Fig. 5h). The less water vapor above PBL is further exacerbated by the updraft associated with the local convergence due to the smoke heating, and hence more water vapor can be seen between 3–6 km. The change of water vapor during night (Fig. 4l) nevertheless can be considered as residual effect from the day. Over ocean (106° E–110° E), the feedback of aerosol yields more low-level convergence (Fig. 4f) and a slightly unstable PBL structure (Fig. 3b), which will be also illustrated in Fig. 7 of Sect. 3.3. Since there is no shortage of water over ocean, the resultant low-level convergence can transport more water vapor upward. Hence, on monthly basis, the water vapor that is uplifted above 2–3 km, may result in an overall increase of precipitable water over the ocean (Fig. 3d) over Karimata strait.

To focus on the area of maximum emissions, the monthly averaged vertical profiles of $PM_{2.5}$ concentration, heating rate, temperature and also the their change due to the smoke radiative feedbacks averaged for all grid boxes over the smoke source region at four different times are represented in Fig. 6. The surface smoke concentration has the minimum in the morning (08:00 LT). The column burden of smoke mass increases rapidly after the fire activity starts in the morning (08:00 LT) and achieves maximum values in the early night (20:00 LT) (Fig. 6a). As PBL progress from morning towards nighttime, with stronger turbulence mixing (and upward motion, Fig. 6c) together with the more intensified fire activities, a well-mixed smoke distribution in the vertical can be found at 16:00 and 20:00 LT within 2 km. The residue effect of smoke to nighttime concentrations (00:00 LT) is obvious within the whole column and more prominent at around 1.5 km. Consistent with our interpretation in Fig. 4, the increase of temperature (ΔT) induced by smoke particles is generally found in 1.5–3 km with peak around 2 km (Fig. 6e), which leads to increase of upward motion at this atltiude range, and more

stability (or overall slight decrease of upward motion) below this altitude (Fig. 6d). Consequently, the increase of $PM_{2.5}$ ($\Delta PM_{2.5}$) is found in 2–3.5 km with peak around 3 km (Fig. 6b); the decrease of $PM_{2.5}$ and T due to smoke radiative effect are found mainly below 2 and 1.5 km respectively during daytime. The staggering feature supports the hypothesis of the secondary circulation (e.g., updraft above boundary layer) introduced by the smoke absorption (as supported by the wind vector change in Fig. 4), although large-eddy simulations at finer scale is further needed to test this hypothesis.

It is worth noting that within $\sim$ 200–300 m above surface, $PM_{2.5}$ concentration is increased in the morning and night, with larger increase during the night (20:00 LT), likely reflecting the effect of reduced PBLH. As discussed above (Fig. 4), different with other times, at 16:00 LT the $PM_{2.5}$ decrease all the way below 2 km. In the morning (08:00 LT), the ΔHeating rate is negative with small magnitude (−0.5 K/day) close to the surface and positive with 0.2 K/day at about 100 m above the surface (Fig. 6e). At afternoon (16:00 LT) the ΔHeating rate is −2 K/day near surface, and above surface it increases from smaller warming to the peak value which is near 6 K/day at $\sim$ 2.5 km. The response of ΔT to the ΔHeating rate involves the heat transfer through turbulent mixing within PBL. At 00:00 LT, ΔT is negative with small magnitude (0.15 K) that appears near the surface due to the residual effect of ΔT in the daytime. In the morning (08:00 LT) as the sunrises, the ΔT is more negative (cooler) near surface and become positive (warming) at $\sim$ 500 m. In the afternoon, in association with the stronger mixing of cooling air from the surface to upper layer, the critical layer at which the ΔT shifts from negative to positive is near 2 km at 16:00 and 20:00 LT.

3.3 Cloud

Over the Maritime Continent cloud cover (Fig. 7a and e) is persistent during both day (denoted as D in all panel captions in Fig. 7) and night (denoted as N). This large cloud cover is primarily contributed by the high-level clouds (6000 m above surface, Fig. 7d and h), although the fraction of low-level cloud (2000 m above surface) is also important, with a monthly average of 0.6 over ocean and 0.25 over land (Fig. 7b and f). The

mid-level cloud over both land area and ocean region is generally below 0.1 (Fig. 7c and g). Because of this small amount of middle-level clouds and also because that smoke are seldom transported to above 6 km in any radiatively appreciable quantity, our analysis focus on the change of low-level cloud ($\Delta\text{Cloud} = \text{Cloud}_{aerosol} - \text{Cloud}_{non-aerosol}$) due to the smoke radiative feedback (third and fourth row in Fig. 7) in both day and night. Indeed, the change of low-level clouds in day (Fig. 7j) and night (Fig. 7n) are both representative of the change of columnar total cloud cover in day and night (Fig. 7i and m). We should notice that the change of cloud here was contributed by the semi-direct effect and did not include the influence from indirect effect since the indirect effect is turn off in all the simulations and is planned for future studies.

Over the Malay Peninsula, Sumatra Island and Borneo Island, the low-level cloud fraction during daytime is decreased by more than 10 % in the simulation (Fig. 7j) likely due to the smoke-induced reduction of evaporation at the surface (Fig. 2d), the increase of atmospheric stability in the boundary layer (Fig. 3b), and the increase of solar heating rate around 2 km (Fig. 6c), all of which are discussed in the previous section. While the sign of change in cloud fraction is consistent with past studies, the amount of change is somewhat less. For example, Korean et al. (2004) reported that scattered cumulus cloud cover over Amazon region can be reduced by 38 % due to smoke semi-direct effects. However, what is unexpected is an increase of cloud cover over a narrow belt region of Karimata Strait and south coastal area of Kalimantan (Fig. 7j). Comparing with the daytime, a distinct difference in nighttime is the increase of cloud fraction over most area of the Karimata Strait and Java Sea (Fig. 7n), and virtually no decrease of cloud fraction in the study region. The increase of cloud fraction in both daytime and nighttime can be attributed to the change of the low-level wind pattern ($\Delta\text{Wind} = \text{Wind}_{aerosol} - \text{Wind}_{non-aerosol}$) (Fig. 7k). During daytime the southeast trade winds increase over most region at south of $-1°$ S (the red shaded area in Fig. 7k), and decrease after crossing the equator (the blue shaded area in Fig. 7k). Consequently, a dynamic low-level convergence is formed over Karimata Strait and south coast of Kalimantan, favoring the low-level cloud formation. In contrast, during

nighttime, a larger area with more convergence and hence increased formation of cloud (Fig. 7n) can be seen over Karimata Strait and also Java Sea.

The contrast of the changes of cloud cover due to the smoke radiative effect between the night and day, and between the ocean and land, reflects the importance to consider the surface properties. Over land, smoke semi-direct effect is important in daytime and it increases stability and saturation water vapor pressure through heating within clouds (Fig. 6f), and so reduces the cloud cover, but has virtually zero effect at night. Over most ocean area, however, the smoke semi-direct effect is much less. The large day-night difference of the responses of columnar cloud fraction to smoke radiative feedback is mainly located in the coastal regions (Fig. 7p), and is primarily contributed by the change of low-level cloud fraction (Fig. 7l). This suggests that the change of sea breeze likely play a role to the change of cloud fraction by extending the offshore convergence zone; the daytime decrease (increase) of low-level (middle-level) air temperature over land weaken the sea breeze, while the nighttime decrease of surface temperature over the land enhance the land breeze.

4   Sensitivity experiments to the OC/BC ratio

By conducting a sensitivity experiment with respect to the change of OC/BC ratio, we can re-examine the processes discussed relative to assumptions about smoke particle absorption. Processes should respond differently to the change of smoke absorption and the resultant change of atmospheric temperature profile. A change the OC/BC ratio from 10 in base case to 3.5 (17) results in a factor of 2 increase (decrease) in the SWDRF (Fig. 8). Smaller OC/BC ratio leads to more warming, while increases of OC/BC ratio leads to more cooling. Indeed, SWDRF is negative over the east part of Karimata Strait for the cases with OC/BC ratio of 17, and close to zero over the most land region. Hence, Fig. 8 verifies that the positive SWDRF in baseline case is due to the absorptive smoke particles within and above the low-level clouds.

While change of OC/BC ratio results in the small change in AOD, it can lead to large differences in AAOD (Fig. 9a). Since the smoke direct radiative effect is a strong function of time of a day, its impacts on the surface energy budget, cloud fraction, and boundary layer height as domain averaged for over the smoke source region are analyzed in terms of their monthly means as a function of local time (Fig. 9). As mentioned in previous sections, over smoke source region, the CCN concentration is likely saturated, and hence the aerosol indirect effect not included in this study might be not as important as semi-direct effect (Koren et al., 2008). However, over the ocean further out from the MC, the smoke indirect effect may increases the cloud albedo, and thereby further enhance the heating by smoke absorption above clouds. Future study is planned and needed to examine how such smoke indirect and semi-direct effects on clouds may influence the solar heating due to smoke particles above the clouds.

Geographically, the changes of aforementioned variables due to the smoke radiative feedbacks are similar as their counterparts in base case. Temporally, SWDRF, ΔGSW, ΔSH, and ΔLH all follow the similar diurnal pattern with peak around local noon (1.00 p.m.) and their magnitude decreases from noon to the morning and evening (Fig. 9b–e); their corresponding values all increase in magnitude by 150 % as OC/BC ratio decreases from 10 to 3.5, and decrease by 50 % as OC/BC ratio increases from 10 to 17. For the base-case, the peak values for SWDRF, ΔGSW, ΔSH, and ΔLH are 9.70 %, 16.19 %, 25.14 %, and 13.06 % of the corresponding values for outgoing TOA SW, GSW, SH, and LH without aerosol feedbacks.

ΔT at 2 m (ΔT2) has dual peaks in 09:00 LT and 18:00 LT (Fig. 9f). As discussed in Wang and Christopher (2006), in early morning and late afternoon when turbulent mixing is weaker, the air warmed by smoke absorption is less effectively transported to the surface and so reduction of T2 peaks (assuming sensible heat flux from the surface remains the same). ΔPBLH has similar diurnal pattern with ΔT2 (Fig. 9g), while the response of PBLH to the decrease of T2 involves the turbulent transport of cool air from the surface to the PBLH, which cause ΔPBLH to lag behind ΔT2.

As discussed in the Sect. 3.2, cloud fraction is reduced during the day and increased during the night. Figure 9h shows that the reduction during day is largest during the late morning time when $\Delta T2$ is minimal, while large increase is close to the midnight. The change of cloud fraction is smaller both during day and night as OC/BC ratio increases, suggesting that the heating by smoke absorption is a key factor that contributes to the change of clouds.

To summarize, averaged quantities with different OC/BC ratio in October 2006 over smoke source region are showed in Fig. 10a. Overall, for the variations of OC/BC ratio from 3.5, to 10, and to 17, AOD has the smallest changes ($< 5\%$), while other variables have larger response especially for the change of OC/BC ratio from 3.5 to 10. A reduction of $\sim 20\%$ can be found for PBLH, T2, CLD, and GSF, LH, and SH, AAOD, and SWDRF when OC/BC ratio is changed from 3.5 to 10. Interesting, net change of cloud fraction is an increase, and such increase gets smaller as aerosols become more scattering (or OC/BC ratio gets larger). Analysis focusing in daytime and night separately shows that this overall increase of cloud fraction is due to the large increase of cloud fraction at night (Fig. 7n). What is shown in Fig. 10a can also be found for a big event in 31 October of 2006 (Fig. 10b). The aerosol radiative impacts in this big event are much prominent compared to the monthly averaged ones and detailed analysis can be seen in Sect. 5.

Figure 11 shows the 30 day averages of vertical distribution of $PM_{2.5}$ concentration, temperature (black line) and the difference (colorful line) of each variable ($V = V_{areosol} - V_{non\text{-}aerosol}$) caused by radiative effect of smoke aerosol with different OC/BC ratios averaged in the smoke source region in October. The change of $PM_{2.5}$ concentration and temperature shows similar pattern for different OC/BC ratio, and the higher concentration of BC always enhances the change. The maximum $PM_{2.5}$ concentration can be found within PBLH (0.6 km above ground). Accordingly, within this averaged PBLH, the aerosol mass increase near surface is $\sim 1.5\,\mu g\,m^{-3}$ for BC/OC of 10 and 17, $\sim 2\,\mu g\,m^{-3}$ for BC/OC of 3.5. The decrease of $PM_{2.5}$ concentration occurs between 0.6 km and 2 km with peak value of $-4\,\mu g\,m^{-3}$ (for BC/OC of 3.5), and $-2.5\,\mu g\,m^{-3}$ (for

BC/OC of 10 and 17) at 1.5 km. Around 3 km above the surface, only slight increase of $PM_{2.5}$ occurs for OC/BC of 17, and the peak value is 2.5 and 3.2 $\mu g\,m^{-3}$ for OC/BC of 10 and 3.5 respectively. Air temperature increases above 1.2 km with the peak value of 0.3 K at 2 km for OC/BC of 3.5, and decreases below 1.2 km with the peak value of −0.4 K at surface for OC/BC value of 3.5. The change of air temperature for OC/BC of 17 and 10 is close, with maximum decrease (−0.25 K) at surface, and the maximum increase of 0.1 K at 2 km. Overall, stronger absorption lead to more stable lower troposphere, with enhancement of aerosol above PBL and near the surface, and reduction of aerosols in middle-to-upper fraction of the PBL.

5 Case study on 31 October 2006

To further illustrate and articulate the smoke radiative feedback to meteorology, Fig. 12 shows the distribution of averaged quantities for the afternoon time during a heavy smoke event during 12:00–16:00 LT on 31 October 2006. During this time period, smoke layers can be found from the true color images (Fig. 12a and b) over Borneo Island, and the corresponding AOD (higher than 2.5) and AAOD (around 0.5) are both much larger than the monthly averaged counterparts (Fig. 12c and d), although the SSA of 0.81 (Fig. 12e) over fire area is similar. Consistent with the pattern of high AOD and low-level cloud distribution (Fig. 12n), large positive value of SWDRF (up to 60 $W\,m^{-2}$) is found over downwind area (Fig. 12f). Right over smoke source area, however, no low-level cloud and relative small aerosol SWDRF are found, which confirms that the low-level cloud is important to cause the positive forcing of smoke aerosols. During such big smoke event, the GSW in the afternoon over fire area can be decreased by 400 $W\,m^{-2}$ from 800 $W\,m^{-2}$ (Fig. 12g), and the resultant reduction of T2 and PBLH can reach to 2 K (from 304 K) and 800 m (from 1600 m) respectively; T increases at 2200 m (Fig. 12i) can be 2 K (much lager than the monthly average value of 0.6 K). At the height of 500 m, the vertical velocity (W) decreases over the center of fire area and increases around the center of fire area. In contrast, at 2200 m (Fig. 12 l and

m) the vertical velocity increases over most fire area. Consistently, surface $PM_{2.5}$ mass concentration increases up to $40\,\mu\mathrm{g\,m^{-3}}$ over fire area and decreases with the similar amount surround the center of fire area (Fig. 12k). The increased solar heating rate above PBLH at afternoon time also plays a dominant role for the change of low-level cloud. Over most the downwind area at Borneo Island the low-level cloud fraction during afternoon time is decreased by 40 % in the simulation (Fig. 12o). Further sensitivity analysis show the more smoke absorption (with OC/BC ratio = 10) amplifies the above proposed mechanisms (Fig. 13).

What is shown for 31 October 2006 can also be found for several other big events in October 2006 (Fig. S1). The aerosol radiative impacts in these big events are much prominent compared to the monthly averaged ones. The change of low-level cloud in all these cases demonstrates the smoke radative feedback on cloud through its change in sea breeze, i.e., an increase of cloud cover due to decrease of sea breeze over the costal water.

6 Conceptual model

Analysis in Sects. 3–5 show that the direct and semi-direct radiative impact (excluding indirect effect) of smoke particles over the Southeast Asian Maritime Continent led to a chain of interesting feedback processes. As illustrated in Fig. 14, these processes have strong difference between day and night, and between land and ocean.

During the daytime in conditions without radiative feedback of aerosols, a local circulation for sea breeze forms between land and ocean, in which air rises over the hotter land surface to form low-level clouds, and air sinks over the ocean to suppress the cloud (Fig. 14a). However, considering the radiative feedback of aerosol particles, the increased solar heating in the atmosphere leads to a net increase of a steady updraft above the boundary layer clouds, which transfers more smoke from boundary layer to the clouds and above and results in a positive feedback; while the decrease of land surface temperature and turbulence lead to decrease of PBLH and the weakening of sea

breeze. The induced updrafts by smoke in turn favor the upward transport and thus lead to decrease of $PM_{2.5}$ in the PBL, albeit the PBLH is decreased. Often in these cases, the capping effect of PBL may not exist (Fig. 4e).

At night, a local circulation of land breeze can be formed, and is enhanced by the decrease of land surface temperature due to smoke radiative feedback during the day. As a result, PBLH decreases, and consequently, $PM_{2.5}$ increases near surface but decreases in the middle-to-upper part of PBL. However, a higher concentration of $PM_{2.5}$ above the cloud layer remains as the residual layer from the daytime. The conceptual model presented in Fig. 14 is further supported by the sensitivity experiments with respect to the change of OC/BC.

Since our numerical experiments are designed to study the smoke semi-direct effect, and also over the Maritime Continent is persistent cloud cover, the change of cloud fraction is another focus of our analysis. Over land, the heating within cloud layers and the increased low-level stability, both due to the absorption of solar radiation by smoke particles, favor the decrease of low-level cloud cover, which can be considered as negative feedback, because the decrease of cloud cover can weak the heating by the smoke particles above. Such smoke semi-direct effect on cloud is important in daytime, but has virtually zero effect at night. Over Karimata Strait, the convergence due to the change of the low-level wind pattern causes increase of cloud fraction in both daytime and nighttime. However, it is also noted that the large day-night difference of the responses of columnar cloud fraction to smoke radiative feedback is mainly located in the coastal regions, and is primarily contributed by the change of low-level cloud fraction. This suggests that the change of sea breeze likely play a role to the change of cloud fraction. This response of coastal wind to the smoke radiative feedback, however, should be considered in the regional context.

A multi-scale analysis of modeling and field campaign data is needed to further evaluate the conceptual model proposed this study. The unique topographical and geographical layout of the Southeast Asian Maritime Continent requires an integrated use

of the data and modeling tools to resolve the processes at the local and regional scales toward a full understanding of smoke direct and indirect effects in that region.

7 Summary and discussions

The direct and semi-direct radiative impact of smoke particles over the Southeast Asian Maritime Continent (MC, 10° S–10° N, 90° E–150° E) during October 2006 were studied in the online-coupled Weather Research and Forecasting model with Chemistry (WRF-Chem). The unique position between absorbing smoke particles and clouds in the vertical led to a chain of interesting interactions between smoke radiative feedback, boundary layer processes, and low level cloud formation in the context of an already interesting meteorological regime that includes the sea breeze and trade winds. Due to the dearth of observation, we are not able to do the comparison with the reality, so most results here only showed the possibilities under the physical mechanism represented in the model. Key findings from this study can be summarized as the following:

1. Persistent and large low-level cloud cover in this region is found to enhance absorption of solar radiation by smoke particles within and above the low-level clouds, and hence results a positive forcing of smoke particles at the top-of-atmosphere, with a monthly and domain averaged value of $\sim 20\,\mathrm{W\,m^{-2}}$ over Borneo and Sumatra and $\sim 60\,\mathrm{W\,m^{-2}}$ during 31 October afternoon over Borneo for OC/BC ratio of 10.

2. The decrease of land surface temperature (up to 1 K for monthly average and 2 K during 31 October afternoon) as a result of smoke radiative extinction of solar input lead to a decrease in turbulence and the PBLH (100 m for monthly average and more than 800 m during 31 October afternoon) and the weakening of sea breeze. The induced updrafts by aerosol above BPL in turn favor the upward turbulent transport and thus lead to the increase of monthly smoke concentration by $\sim 4\,\mathrm{\mu g\,m^{-3}}$ (monthly afternoon time can increase $\sim 10\,\mathrm{\mu g\,m^{-3}}$) over 2–3.5 km.

Surface $PM_{2.5}$ of monthly afternoon time showed smaller increased right over the center of fire area, and increase up to $40\,\mu g\,m^{-3}$ during 31 October afternoon time. At night, land breeze is enhanced by the decrease of land surface temperature due to smoke radiative feedback during daytime.

5   3. Over land, smoke semi-direct effect is important in daytime and it increases stability and reduces the cloud cover, but has virtually zero effect at night. This reduction in cloud cover represents a negative feedback with smoke particle absorption above. Over Peninsula Malaysia, Sumatra Island and Borneo Island, the monthly averaged low-level cloud fraction during daytime is decreased by more
10   than 10 % and 40 % decreased can be found over Borneo during 31 October afternoon. Over Karimata Strait, the change of the low-level wind pattern induced the convergence cause increase of cloud fraction in both daytime and nighttime. The decreased sea breeze during afternoon time can lead to prominent increase (40 %) of low-level cloud over coastal water.

15   **Supplementary material related to this article is available online at: http://www.atmos-chem-phys-discuss.net/13/15443/2013/ acpd-13-15443-2013-supplement.pdf.**

References

Akagi, S. K., Yokelson, R. J., Wiedinmyer, C., Alvarado, M. J., Reid, J. S., Karl, T., Crounse, J. D., and Wennberg, P. O.: Emission factors for open and domestic biomass burning for use in

atmospheric models, Atmos. Chem. Phys., 11, 4039–4072, doi:10.5194/acp-11-4039-2011, 2011.

Barnard, J. C., Fast, J. D., Paredes-Miranda, G., Arnott, W. P., and Laskin, A.: Technical Note: Evaluation of the WRF-Chem "Aerosol Chemical to Aerosol Optical Properties" Module using data from the MILAGRO campaign, Atmos. Chem. Phys., 10, 7325–7340, doi:10.5194/acp-10-7325-2010, 2010.

Bond, T. C. and Bergstrom, R. W.: Light absorption by carbonaceous particles: an investigative review, Aerosol Sci. Tech., 40, 27–67, 2006.

Chang, H. and Charalampopoulos, T. T.: Determination of the wavelength dependence of refractive indices of flame soot, P. R. Soc. Lond. Ser. A, 430, 577–591, 1990.

Campbell, J. R., Reid, J. S., Westphal, D. L., Zhang, J., Tackett, J. L., Chew, B. N., Welton, E. J., Shimizu, A., and Sugimoto, N.: Characterizing aerosol particle composition and the vertical profile of extinction and linear depolarization over Southeast Asia and the Maritime Continent: the 2007–2009 view from CALIOP, Atmos. Res., 122, 520–543, 2011b.

Chapman, E. G., Gustafson Jr., W. I., Easter, R. C., Barnard, J. C., Ghan, S. J., Pekour, M. S., and Fast, J. D.: Coupling aerosol-cloud-radiative processes in the WRF-Chem model: Investigating the radiative impact of elevated point sources, Atmos. Chem. Phys., 9, 945–964, doi:10.5194/acp-9-945-2009, 2009.

Colarco, P., Schoeberl, M., Doddridge, B., Marufu, L., Torres, O., and Welton, E.: Transport of smoke from Canadian forest fires to the surface near Washington, DC: injection height, entrainment, and optical properties, J. Geophys. Res, 109, D06203, doi:(10.1029/2003JD004248), 2004.

Davison, P. S., Roberts, D. L., Arnold, R. T., and Colvile, R. N.: Estimating the direct radiative forcing due to haze from the 1997 forest fires in Indonesia, J. Geophys. Res., 109, D10207, doi:10.1029/2003JD004264, 2004.

Fast, J. D., Gustafson Jr, W. I., Easter, R. C., Zaveri, R. A., Barnard, J. C., Chapman, E. G., Grell, G. A., and Peckham, S. E.: Evolution of ozone, particulates, and aerosol direct radiative forcing in the vicinity of Houston using a fully coupled meteorology-chemistry-aerosol model, J. Geophys. Res., 111, D21305, doi:10.1029/2005JD006721, 2006.

Feng, N. and Christopher, S. A.: Satellite and surface-based remote sensing of Southeast Asian aerosols and their radiative effects, Atmos. Res., 122, 544–554, doi:10.1016/j.atmosres.2012.02.018, 2012.

Discussion Paper | Discussion Paper | Discussion Paper | Discussion Paper | Discussion Paper

Ghan, S. J., Laulainen, N. S., Easter, R. C., Wagener, R., Nemesure, S., Chapman, E. G., Zhang, Y., and Leung, L. R.: Evaluation of aerosol direct radiative forcing in MIRAGE, J. Geophys. Res., 106, 5295–5316, 2001a.

Grell, G., Freitas, S. R., Stuefer, M., and Fast, J.: Inclusion of biomass burning in WRF-Chem: impact of wildfires on weather forecasts, Atmos. Chem. Phys., 11, 5289–5303, doi:10.5194/acp-11-5289-2011, 2011.

Grell, G. A. and Dévényi, D.: A generalized approach to parameterizing convection combining ensemble and data assimilation techniques, Geophys. Res. Lett., 29, 1693, doi:10.1029/2002GL015311, 2002.

Grell, G. A., Peckham, S. E., Schmitz, R., McKeen, S. A., Frost, G., Skamarock, W. C., and Eder, B.: Fully coupled "online" chemistry in the WRF model, Atmos. Environ., 39, 6957–6975, 2005.

Haywood, J. M. and Ramaswamy, V.: Global sensitivity studies of the direct radiative forcing due to anthropogenic sulfate and black carbon aerosols, J. Geophys. Res., 103, 6043–6058, 1998.

Haywood, J. M. and Shine, K. P.: Multi-spectral calculations of the direct radiative forcing of tropospheric sulphate and soot aerosol using a column model, Q, J. Rroy. Meteorol. Soc., 123, 1907–1930, 1997.

Heintzenberg, J., Charlson, R. J., Clarke, A. D., Liousse, C., Ramaswamy, V., Shine, K. P., Wendisch, M., and Helas, G.: Measurements and modeling of aerosol single scattering albedo: progress, problems and prospects, Contrib. Atmos. Phys., 70, 249–263, 1997.

Herner, J. D., Aw, J., Gao, O., Chang, D. P., and Kleeman, M. J.: Size and composition distribution of airborne particulate matter in northern California: I – particulates mass, carbon, and water-soluble ions, J. Air Waste Manage., 55, 30–51, 2005.

Hong, S.-Y. and Kim, S.-W.: Stable boundary layer mixing in a vertical diffusion scheme, in: Proceedings of Ninth Annual WRF User's Workshop, Boulder, CO, National Center for Atmospheric Research, 3.3., available at http://www.mmm.ucar.edu/wrf/users/workshops/WS2008/abstracts/3-03.pdf, 2008.

Hyer, E. J. and Chew, B. N.: Aerosol transport model evaluation of an extreme smoke episode in Southeast Asia, Atmos. Environ., 44, 1422–1427, 2010.

Hyer, E. J., Reid, J. S., Prins, E. M., Hoffman, J. P., Schmidt, C. C., Miettinen, J. I., and Giglio, L.: Patterns of fire activity over Indonesia and Malaysia from polar and geostationary satellite observations, Atmos. Res., 122, 504–519, doi:10.1016/j.atmosres.2012.06.011, 2013.

Mesoscale modeling of smoke transport

C. Ge et al.

Hu, X. M., Nielsen-Gammon, J. W., and Zhang, F.: Evaluation of three planetary boundary layer schemes in the WRF model, J. Appl. Meteorol. Clim., 49, 1831–1844, 2010.

IPCC: Climate Change 2007: The Physical Science Basis. Contribution of Working Group I to the Fourth Assessment. Report of the Intergovernmental Panel on Climate Change edited by: Solomon, S., D. Qin, M. Manning, Z. Chen, M. Marquis, K. B. Averyt, M. Tignor and Miller, H. L., Cambridge University Press, Cambridge, UK, New York, NY, USA, 996 pp., 2007.

Jacobson, M. Z.: . A physically-based treatment of elemental carbon optics: implications for dlobal direct forcing of aerosols, Geophys. Res. Lett., 27, 217–220 , 2000.

Johnson, G. C., Lyman, J. M., Willis, J. K., Levitus, S., Boyer, T., Antonov, J., and Good, S. A.: (Global oceans) Ocean heat content (in "State of the Climate in 2011"), B. Am. Meteorol. Soc., 93, S62–S65, 2012.

Kanakidou, M., Seinfeld, J. H., Pandis, S. N., Barnes, I., Dentener, F. J., Facchini, M. C., Van Dingenen, R., Ervens, B., Nenes, A., Nielsen, C. J., Swietlicki, E., Putaud, J. P., Balkanski, Y., Fuzzi, S., Horth, J., Moortgat, G. K., Winterhalter, R., Myhre, C. E. L., Tsigaridis, K., Vignati, E., Stephanou, E. G., and Wilson, J.: Organic aerosol and global climate modelling: a review, Atmos. Chem. Phys., 5, 1053–1123, doi:10.5194/acp-5-1053-2005, 2005.

Kondo, Y., Matsui, H., Moteki, N., Sahu, L., Takegawa, N., Kajino, M., Zhao, Y., Cubison, M., Jimenez, J., and Vay, S.: Emissions of black carbon, organic, and inorganic aerosols from biomass burning in North America and Asia in 2008, J. Geophys. Res., 116, D08204, doi:10.1029/2010JD015152, 2011.

Koren, I., Kaufman, Y. J., Remer, L. A., and Martins, J. V.: Measurement of the effect of Amazon smoke on inhibition of cloud formation, Science, 303, 1342–1345, 2004.

Koren, I., Martins, J. V., Remer, L. A., and Afargan, H.: Smoke invigoration versus inhibition of clouds over the Amazon, Science, 321, 946–949, 2008.

Levitus, S., Antonov, J. I., Boyer, T. P., Baranova, O. K., Garcia, H. E., Locarnini, R. A., Mishonov, A. V., Reagan, J. R., Seidov, D., Yarosh, E. S., and Zweng, M. M.: World ocean heat content and thermosteric sea level change (0–2000 m), 1955–2010, Geophys. Res. Lett., 39, L10603, doi:10.1029/2012GL051106, 2012.

Li, W., Luo, C., Wang, D., and Lei, T.: Diurnal variations of precipitation over the South China Sea, Meteorol. Atmos. Phys, 109, 33–46, 2010.

Lim, H.-J., and Turpin, B. J.: Origins of primary and secondary organic aerosol in atlanta: results of time-resolved measurements during the atlanta suxpersite experiment, Environ. Sci. Technol., 36, 4489–4496, 2002.

Mlawer, E. J., Taubman, S. J., Brown, P. D., Iacono, M. J., and Clough, S. A.: Radiative transfer for inhomogeneous atmospheres: RRTM, a validated correlated k-model for the longwave, J. Geophys. Res., 102, 16663–16682, doi:10.1029/97JD00237, 1997.

Mughal, S. M., Yousuff, M., Hussaini, M., Goodrick, S., and Cunningham, P.: Role of buoyancy and heat release, in: Fire Modeling, Propagation, and Instability, edited by: Butler, B., W and Cook, W., The fire environment innovations, management, and policy, Destin, FL. Proceedings RMRS-P-46CD. Fort Collins, CO: US Department of Agriculture, Forest Service, Rocky Mountain Research Station. CD-ROM, 195–219, 2007.

Page, S. E., Siegert, F., Rieley, J. O., Boehm, H.-D. V., Jaya, A., and Limin, S.: The amount of carbon released from peat and forest fires in Indonesia during 1997, Nature, 420, 61–65, doi:10.1038/nature01131, 2002.

Ramanathan, V.: The role of ocean-atmosphere interactions in the CO2 climate problem, J. Atmos. Sci., 38, 918–930, 1981.

Reid, J. S., Hobbs, P. V., Ferek, R. J., Blake, D. R., Martins, J. V., Dunlap, M. R., and Liousse, C.: Physical, chemical, and optical properties of regional hazes dominated by smoke in Brazil, J. Geophys. Res., 103, 32059–32080, doi:10.1029/98JD00458, 1998.

Reid, J. S., Koppmann, R., Eck, T. F., and Eleuterio, D. P.: A review of biomass burning emissions part II: intensive physical properties of biomass burning particles, Atmos. Chem. Phys., 5, 799–825, doi:10.5194/acp-5-799-2005, 2005a.

Reid, J. S., Eck, T. F., Christopher, S. A., Koppmann, R., Dubovik, O., Eleuterio, D. P., Holben, B. N., Reid, E. A., and Zhang, J.: A review of biomass burning emissions part III: intensive optical properties of biomass burning particles, Atmos. Chem. Phys., 5, 827–849, doi:10.5194/acp-5-827-2005, 2005b.

Reid, J. S., Xian, P., Hyer, E. J., Flatau, M. K., Ramirez, E. M., Turk, F. J., Sampson, C. R., Zhang, C., Fukada, E. M., and Maloney, E. D.: Multi-scale meteorological conceptual analysis of observed active fire hotspot activity and smoke optical depth in the Maritime Continent, Atmos. Chem. Phys., 12, 2117–2147, doi:10.5194/acp-12-2117-2012, 2012.

Reid, J. S., Hyer, E. J., Johnson, R., Holben, B. N., Yokelson, R. J., Zhang, J., Campbell, J. R., Christopher, S. A., Di Girolamo, L., Giglio, L., Holz, R. E., Kearney, C., Miettinen, J., Reid, E. A., Joseph, Turk, F., Wang, J., Xian, P., Zhao, G., Balasubramanian, R.,

Chew, B. N., Janai, S., Lagrosas, N., Lestari, P., Lin, N.-H., Mahmud, M., Nguyen, X. A., Norris, B., Oahn, T. K., Oo, M., Salinas, S. V., Welton, E. J., and Liew, S. C.: Observing and understanding the Southeast Asian aerosol system by remote sensing: an initial review and analysis for the Seven Southeast Asian Studies (7SEAS) program., Atmos. Res., 122, 403–468, 2013.

Rosen, H., Hansen, A. D. A., Gundel, L., and Novakov, T.: Identification of the optically absorbing component in urban aerosols, Appl. Optics, 17, 3859–3861, doi:10.1364/AO.17.003859, 1978.

Sahu, L. K., Kondo, Y., Miyazaki, Y., Pongkiatkul, P., and Kim Oanh, N. T.: Seasonal and diurnal variations of black carbon and organic carbon aerosols in Bangkok, J. Geophys. Res., 116, D15302, doi:10.1029/2010JD015563, 2011.

Salinas, S. V., Chew, B. N., Miettinen, J., Campbell, J. R., Welton, E. J., Reid, J. S., Yu, L. E., and Liew, S. C.: Physical and optical characteristics of the October 2010 haze event over Singapore: a photometric and lidar analysis, Atmos. Res., 122, 555–570, 2013.

See, S., Balasubramanian, R., and Wang, W.: A study of the physical, chemical, and optical properties of ambient aerosol particles in Southeast Asia during hazy and nonhazy days, J. Geophys. Res., 111, D10S08, doi:10.1029/2005JD006180, 2006.

Spencer, M. and Prather, K.: Using ATOFMS to determine OC/EC mass fractions in particles, Aerosol Sci. Tech., 40, 585–594, 2006.

Tosca, M. G., Randerson, J. T., Zender, C. S., Nelson, D. L., Diner, D. J., and Logan, J. A.: Dynamics of fire plumes and smoke clouds associated with peat and deforestation fires in Indonesia, J. Geophys. Res., 116, D08207, doi:10.1029/2010JD015148, 2011.

Wang, J. and Christopher, S.: Mesoscale modeling of Central American smoke transport to the United States: 2. Smoke radiative impact on regional surface energy budget and boundary layer evolution, J. Geophys. Res., 111, 1–17, 2006.

Wang, J., Gei, C., Yang, Z., Hyer, E. J., Reid, J. S., Chew, B. N., and Mahmud, M.: Mesoscale modeling of smoke transport over the Southeast Asian Maritime Continent: interplay of sea breeze, trade wind, typhoon, and topography, Atmos. Res., 122, 486–503, 2013.

Wu, L., Su, H., and Jiang, J. H.: Regional simulations of deep convection and biomass burning over South America: 1. Model evaluations using multiple satellite data sets, J. Geophys. Res., 116, D17208, doi:10.1029/2011JD016105, 2011.

Xian, P., Reid, J. S., Atwood, S. A., Johnson, R. S., Hyer, E. J., Westphal, D. L., and Sessions, W.: Smoke aerosol transport patterns over the Maritime Continent, Atmos. Res., 122, 469–485, 2012.

Yu, S., Kasibhatla, P. S., Wright, D. L., Schwartz, S. E., McGraw, R., and Deng, A.: Moment-based simulation of microphysical properties of sulfate aerosols in the eastern United States: model description, evaluation, and regional analysis, J. Geophys. Res., 108, 4353, doi:10.1029/2002JD002890, 2003.

Zhang, Y.: Online-coupled meteorology and chemistry models: history, current status, and outlook, Atmos. Chem. Phys., 8, 2895–2932, doi:10.5194/acp-8-2895-2008, 2008.

Table 1. Configuration Options Employed by WRF-chem in this study.

Atmospheric Process	Model Option
Longwave radiation	RRTM scheme (Mlawer, 1997)
Shortwave radiation	GSFCSW model
Surface layer	MM5
Land surface	Noah
Boundary layer	YSU (Hong, 2006)
Cumulus clouds	G3 (Grell, 2002)
Cloud microphysics	Lin (Lin et al., 1983)
Gas-phase chemistry	RADM2 (Stockwell et al., 1990)
Aerosol chemistry	MADE/SORGAM (Ackermann et al., 1998; Schell et al., 2001).
Optical module	Maxwell-Garnet mixing rule (Barnard et al., 2010)
Horizontal resolution	81 km for outer domain, 27 km for inner domain (Fig. 1)
Vertical layers	27

Table 2. Experiments design.

	Baseline	S1	S2	S3
OC/BC	10	3.5	17	10
BC/particle mass	5.6 %	15.6 %	3.3 %	5.6 %
feedback	yes	yes	yes	no
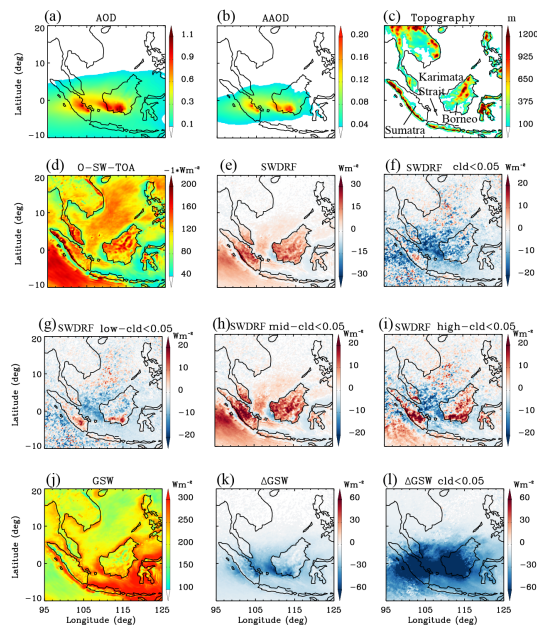
Fig. 1. Distribution of monthly averaged quantities in October 2006. **(a)** Aerosol Optical Depth (AOD), **(b)** Aerosol Absorption Optical Depth (AAOD), **(c)** topography in meter, **(d)** Outgoing Short Wave (SW) at Top of Atmosphere (TOA), O-SW-TOA, **(e)** Aerosol Short Wave Direct Radiative Forcing (SWDRF) at TOA, **(f)** Aerosols SWDRF at TOA for column cloud fraction less than 0.05, **(g)**–**(i)** are similar to **(f)** but respectively for low-level, mid-level, and high-level cloud fractions less than 0.05. **(j)** Net Short Wave flux at the ground (GSW), **(k)** difference of GSW (ΔGSW), **(l)** ΔGSW for cloud fraction less than 0.05. The difference of each variable (ΔV) is defined as $\Delta V = V_{\text{aerosol}} - V_{\text{non-aerosol}}$. The OC/BC ratio is 10 in the simulation.
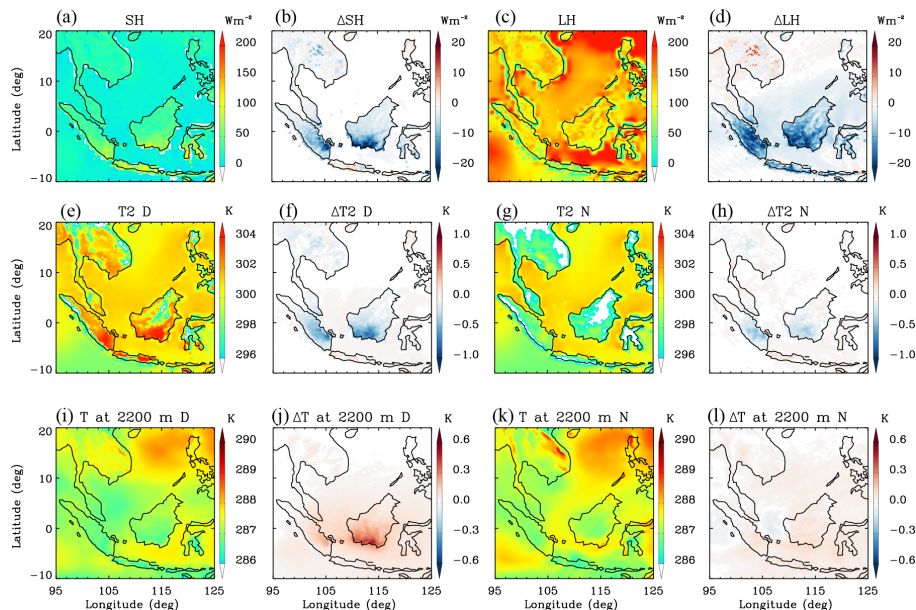
Fig. 2. Distribution of monthly averaged quantities in October 2006. **(a)** Sensible heat flux at the surface (SH) without consideration of smoke radiative feedback, **(b)** difference of SH (ΔSH) due to the smoke radiative feedback. **(c)** and **(d)**, **(e)** and **(f)**, **(g)** and **(h)**, **(i)** and **(j)**, **(k)** and **(l)** are all paired similarly as the pair of **(a)** and **(b)** but for latent heat (LH), 2 m air temperature at daytime, 2 m air temperature at night, temperature at 2.2 km above terrain at daytime, and temperature at 2.2 km above terrain at nighttime, respectively. The difference of each variable (ΔV) is defined as $\Delta V = V_{\text{aerosol}} - V_{\text{non-aerosol}}$. D donates daytime, i.e., the time period between 08:00 LT and 19:00 LT, and N donates nighttime, i.e., between 20:00 LT and 07:00 LT. The simulated results are for the OC/BC ratio of 10.
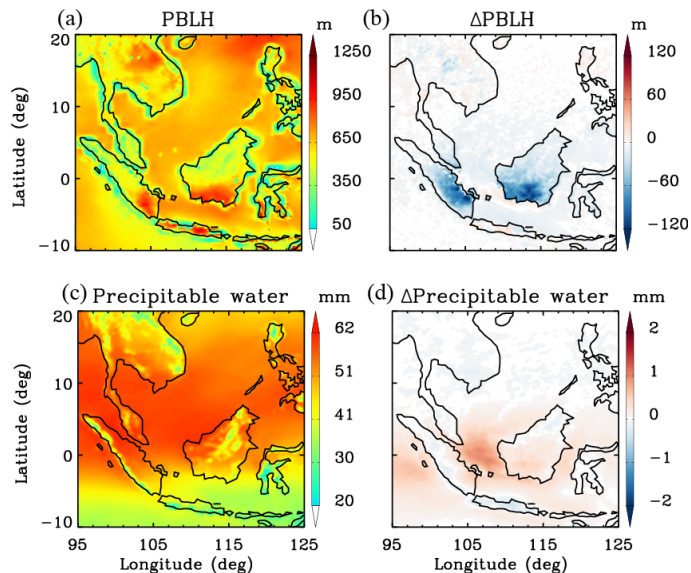
Fig. 3. Distribution of monthly averaged variable in October 2006. **(a)** Planetary boundary layer height (PBLH) without considering the radiative feedback of smoke aerosols, **(b)** difference of PBLH due to the radiative feedback of smoke aerosols. **(c)** and **(d)** are respectively same as **(a)** and **(b)** but for precipitable water. The simulated results are for the OC/BC ratio of 10.

Title Page

Abstract | Introduction

Conclusions | References

Tables | Figures

|◀ | ▶|

◀ | ▶

Back | Close

Full Screen / Esc

Printer-friendly Version

Interactive Discussion
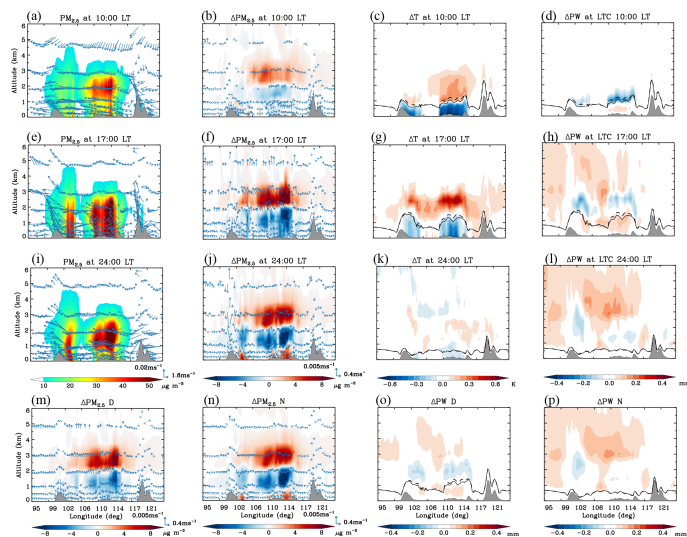
Fig. 4. Top row: vertical cross section of monthly averages in October 2006 at 10.00 a.m. for: **(a)** $PM_{2.5}$ and wind speed, **(b)** change of $PM_{2.5}$, $\Delta PM_{2.5}$, **(c)** change of temperature, ΔT, and **(d)** change of precipitable water ΔPW. Second and third row are respectively the same as the top row but at 5.00 p.m. and 12.00 p.m., respectively. Bottom row: **(m)** and **(n)** show the change of monthly averaged $PM_{2.5}$ at daytime and night time, denoted as $\Delta PM_{2.5}D$ and $\Delta PM_{2.5}N$ respectively. **(o)** and **(p)** are similar as **(m)** and **(n)** but for precipitable water. All variables are averaged along the vertical cross section centered at the latitude of 1° S (extends 5 grid points into and out). The terrain is showed as gray shaded in each panel. Also overlaid in each panel are the PBLH simulated with the feedback of smoke aerosols (black line) and PBLH without feedback of fires (dotted line). The difference of each variable (ΔV) is defined as $\Delta V = V_{aerosol} - V_{non\text{-}aerosol}$. The simulated results are for the OC/BC ratio of 10.
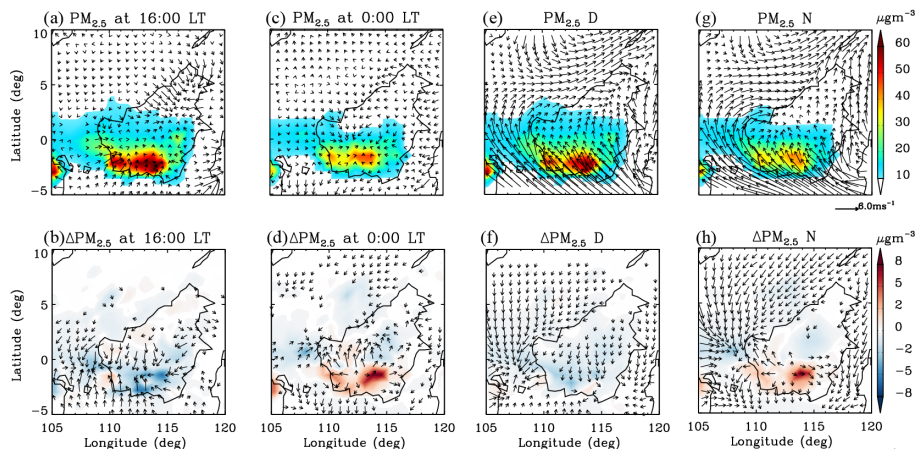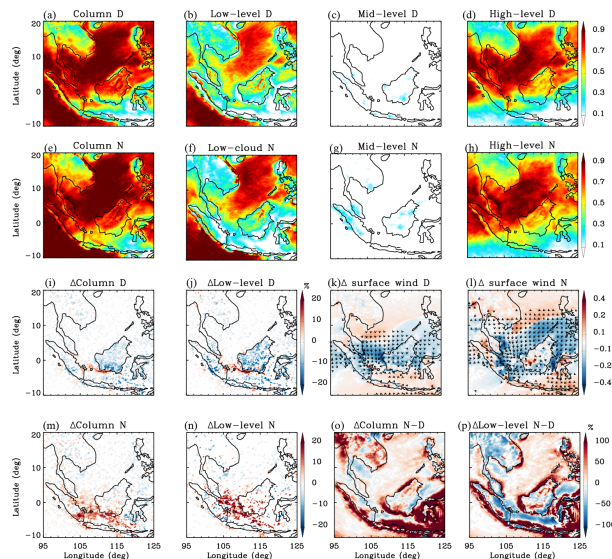
Fig. 5. Distribution of monthly averaged quantities in October 2006. Anomaly of surface wind and monthly averages of $PM_{2.5}$ as a function of local times respectively at **(a)** 16:00 LT, **(c)** 00:00 LT. Difference of surface wind anomaly and $PM_{2.5}$ in monthly averages due to smoke radiative feedback at **(b)** 16:00 LT, and **(d)** 00:00 LT. **(e)** and **(g)** show respectively the monthly averaged surface wind and $PM_{2.5}$ at daytime (denoted as D in panel caption) and nighttime (denoted as N). **(f)** and **(h)** are similarly as counterparts in **(e)** and **(b)** but for difference of monthly averaged surface wind and $PM_{2.5}$ due to smoke radiative feedback. The simulated results are for the OC/BC ratio of 10.

Title Page

Abstract | Introduction

Conclusions | References

Tables | Figures

|◄ | ►|

◄ | ►

Back | Close

Full Screen / Esc

Printer-friendly Version

Interactive Discussion
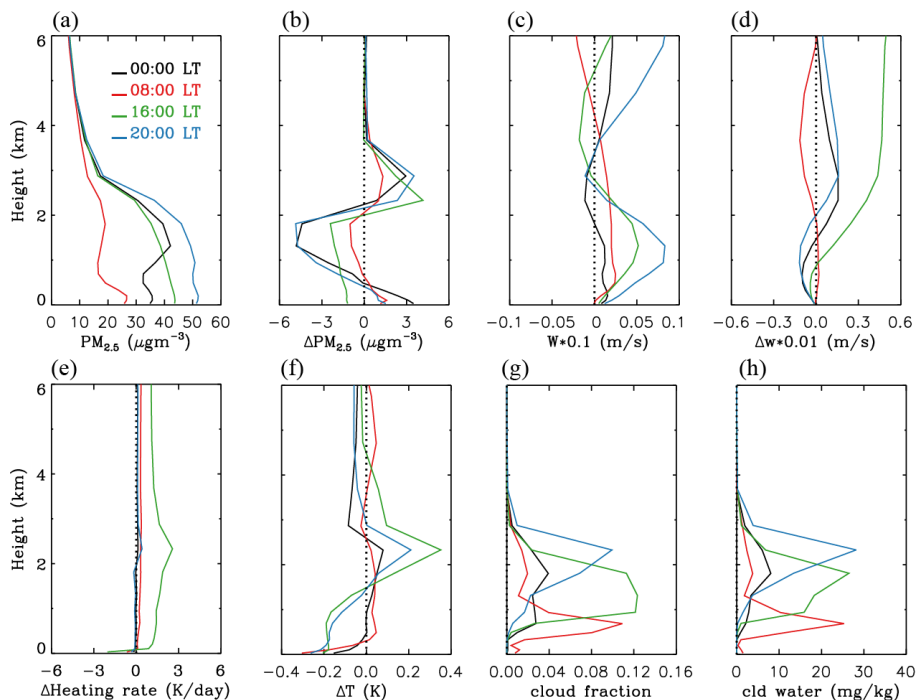
Fig. 6. Vertical distribution of monthly- and domain- averages over the smoke source in October 2006 at different local times for: **(a)** $PM_{2.5}$ concentration, **(b)** difference of $PM_{2.5}$ concentration ($\Delta PM_{2.5}$), **(c)** vertical velocity (w), **(d)** difference of w (Δw), **(e)** difference of heating rate, **(f)** difference of air temperature (ΔT), **(g)** cloud fraction, **(h)** cloud water. The difference of each variable (ΔV) is defined as $\Delta V = V_{aerosol} - V_{non-aerosol}$. The simulated results are for the OC/BC ratio of 10.

Fig. 7. Distribution of monthly averaged quantities in October 2006. Top-row is for simulated daytime **(a)** cloud fraction, **(b)** low level cloud fraction, **(c)** mid-level cloud fraction, and **(d)** high-level cloud, all without consideration of smoke radiative feedback. Second row from the top is the same as top row but for nighttime. Third row from the top shows the differences due to the consideration of smoke radiative feedback for **(i)** cloud fraction, **(f)** low-level cloud fraction, and **(k)** surface wind speed. In the bottom row, **(m)**, **(n)**, and **(o)** are respectively the same as **(i)**, **(i)**, and **(k)** for nighttime. Also shown in **(l)** are the difference between **(j)** and **(n)**, and in **(p)** the difference between **(i)** and **(m)**. All the difference showed here are with 95 % confidence by paired samples t test. Clouds below 2000 m are considered low-level clouds, between 2000 m and 6000 m are middle-level clouds, and above 6000 m are high-level clouds. Note in panel **(k)** and **(o)**, the color filled contours represent the wind speed. Daytime (D) here is the time period between 08:00 LT and 19:00 LT, nighttime (N) is the time between 20:00 LT and 07:00 LT. The simulated results are for the OC/BC ratio of 10.
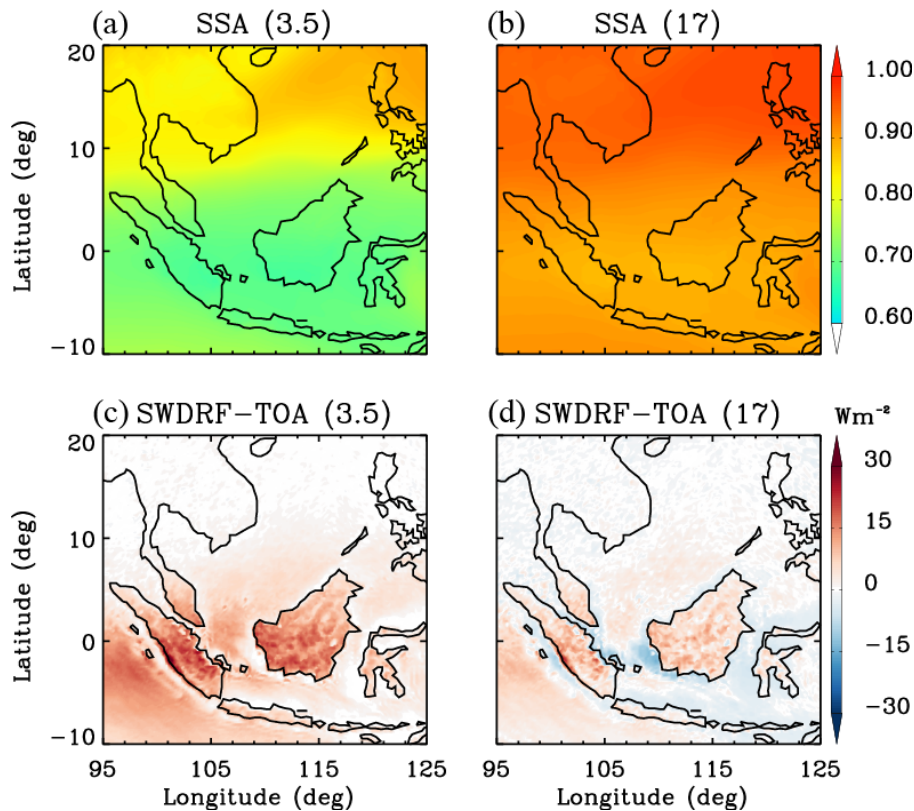
Fig. 8. Distribution of monthly averaged quantities in October 2006 for **(a)** Single scattering albedo (SSA) with OC/BC ratio 3.5, **(b)** SSA with OC/BC ratio as 17, **(c)** SWDRF with OC/BC ratio 3.5, **(d)** SWDRF with OC/BC ratio 17.
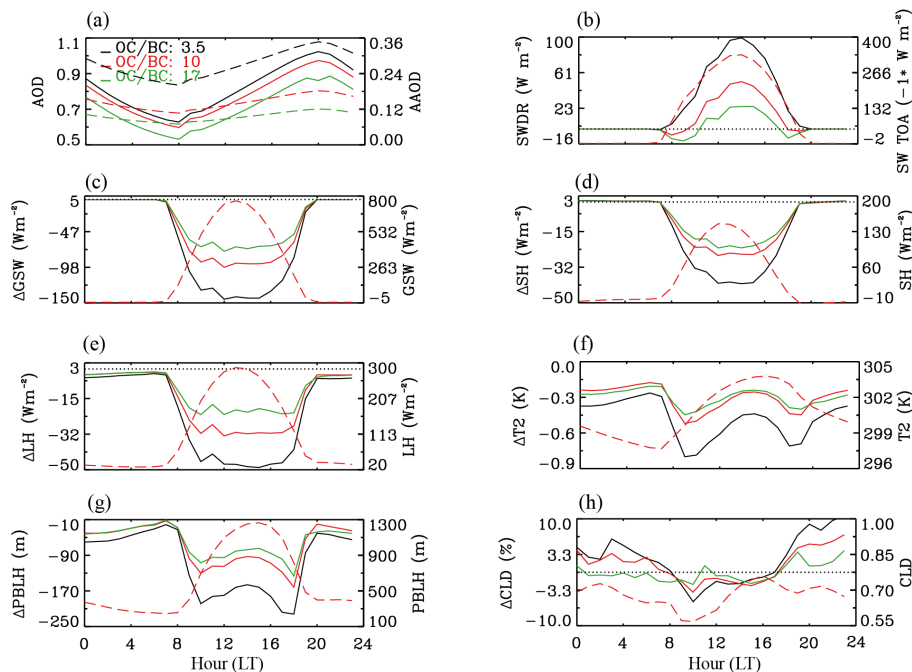
Fig. 9. Monthly- and domain-averaged diurnal variations over the smoke source region in October of 2006 for the following variables simulated by WRF-chem with different OC/BC ratios used in the smoke emission. **(a)** Aerosol optical depth (AOD, solid line) and absorption aerosol optical depth (AAOD, dotted line), **(b)** short wave direct radiative forcing (SWDRF, solid line), outgoing short wave radiation flux at TOA (SW TOA, dotted line), **(c–h)** net short wave flux at surface (GSW), sensible heat flux at the surface (SH), latent heat (LH), 2 m air temperature (T2), planet boundary (PBLH), and cloud fraction (CLD). The dotted lines show variation of the variable (*V*), and the solid lines (with different colors) show the difference of the variable ($\Delta V = V_{\text{areosol}} - V_{\text{non-aerosol}}$) for different OC/BC ratios.

Title Page

Abstract | Introduction

Conclusions | References

Tables | Figures

|◄ | ►|

◄ | ►

Back | Close

Full Screen / Esc
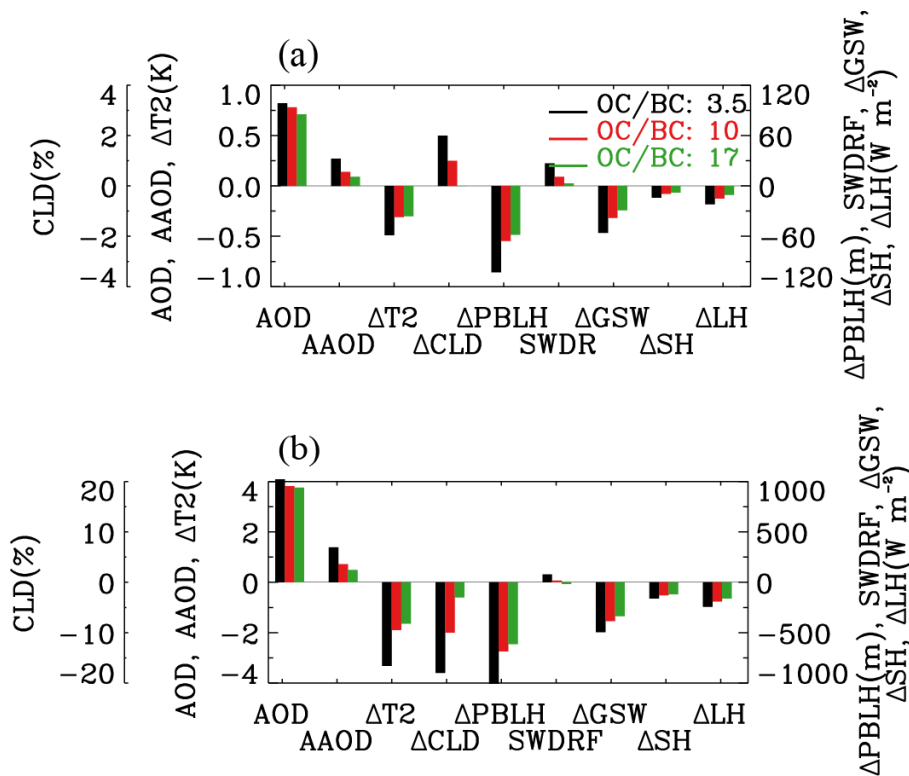
Printer-friendly Version

Interactive Discussion

Fig. 10. (a) Monthly- and domain-averages over the smoke source region simulated with different OC/BC ratios in October of 2006 for AOD, AAOD, as well as the change of T2, PBLH, GSW, SWDR, LH, SH, CLD due to the consideration of smoke radiative effect. The change of each variable is defined as the difference between the simulation with and without the feedback of smoke aerosol ($\Delta V = V_{areosol} - V_{non-aerosol}$). (b): same as (a) but for hourly averages of the daytime (08:00–17:00 LT) in 7 October 2006.

Discussion Paper | Discussion Paper | Discussion Paper | Discussion Paper

Title Page

Abstract | Introduction

Conclusions | References

Tables | Figures

|◄ | ►|

◄ | ►

Back | Close

Full Screen / Esc

Printer-friendly Version
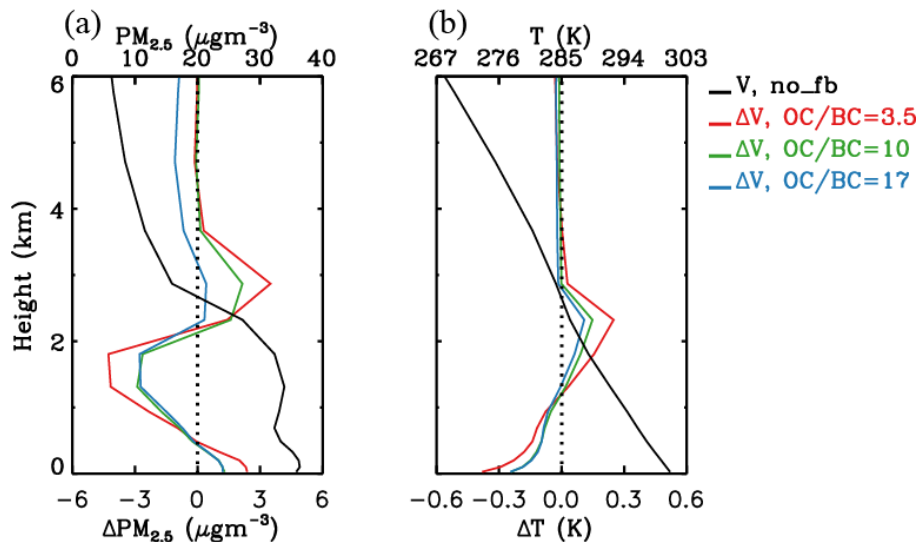
Interactive Discussion

Fig. 11. Vertical distribution of monthly- and domain-averages over the smoke source region in October 2006 for the following variables simulated by WRF-chem with different OC/BC ratios: **(a)** PM$_{2.5}$ concentration, **(b)** air temperature. The black line is the variable (V), and the other lines in different colors show the difference of the variable due to smoke ($\Delta V = V_{\text{areosol}} - V_{\text{non-aerosol}}$) with different OC/BC ratios.
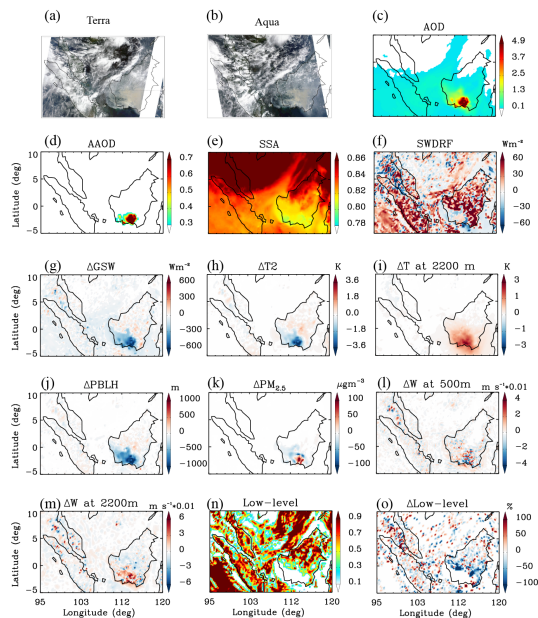
Fig. 12. Distribution of averaged quantities for the afternoon time (12:00–16:00 LT) during a smoke event in 31 October in 2006. **(a)** and **(b)**: MODIS three-band color overlay images (red, band 1; green, band 4; and blue, band 3) from Terra and Aqua satellites, respectively. **(c)** AOD, **(d)** AAOD, **(e)** SSA, **(f)** Aerosol SWDRF at TOA, **(g)** ΔGSW, **(h)** ΔT2, **(i)** ΔT at 2200 m above surface, **(j)** ΔPBLH, **(k)** $\Delta PM_{2.5}$, **(l)** ΔW (vertical velocity) at 500 m above surface, **(m)** ΔW at 2200 m above surface, **(n)** low-level cloud fraction, **(o)** the difference of low-level cloud fraction. The difference of each variable (ΔV) is defined as $\Delta V = V_{\text{aerosol}} - V_{\text{non-aerosol}}$. The OC/BC ratio is 10 in the simulation (BC accounts for 5.6 % smoke particle dry mass).
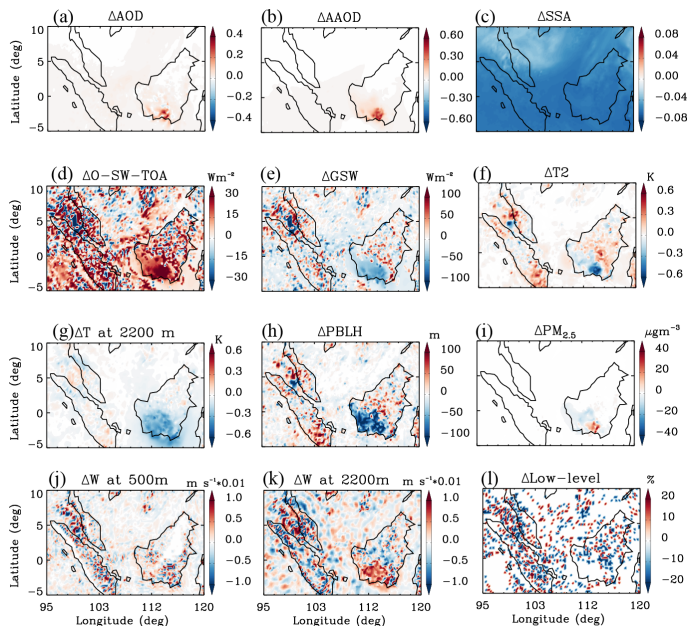
Fig. 13. Similar as Fig. 12 but show the difference of following variables due to changes of smoke absorption: **(a)** Aerosol Optical Depth (AOD), **(b)** Aerosol Absorption Optical Depth (AAOD), **(c)** Single scattering albedo (SSA), **(d)** Outgoing Short Wave (SW) at Top of Atmosphere (TOA), O-SW-TOA, **(e)** Aerosol Short Wave Direct Radiative Forcing (SWDRF) at TOA, **(f)** Net Short Wave flux at the ground (GSW), **(g)** difference of GSW (ΔGSW), **(h)** difference of 2 m air temperature (Δ2T), **(i)** difference of temperature at 2.2 km above terrain (ΔT), **(j)** difference of PBLH (ΔPBLH), **(k)** difference of PM$_{2.5}$ (ΔPM$_{2.5}$), **(l)** difference of vertical velocity (Δw) at 500 m, **(m)** Δw at 2200 m, **(n)** low level cloud fraction, **(o)** difference of low-level cloud fraction. The difference of each variable (ΔV) is defined as ΔV = V$_{oc/bc=10}$ − V$_{oc/bc=17}$.
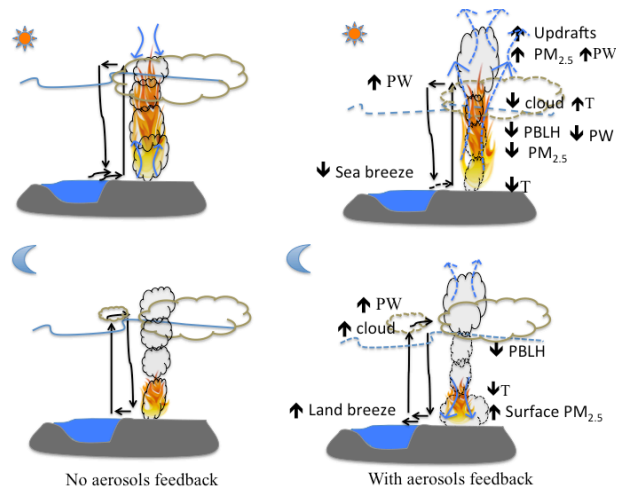
Fig. 14. A conceptual model that illustrates the radiative feedbacks of smoke aerosols on the change of aerosol concentration, PBLH, wind, and cloud fraction over Southeast Asian Marine Continents. Panels on the left show normal conditions without smoke radiative feedback, and on the right shows with changes of different variables due to aerosol radative feedback. During daytime (top row), the smoke-induced local convergences over the smoke source region, which transport more smoke particles above, and hence rendering a positive feedback. During nighttime, however, this elevated smoke layer is decoupled from boundary layer, and the reduction of boundary layer height lead to the increase of smoke particles near the surface. The cloud change over continents are mostly occurred during the daytime over fire area, where the low-level cloud fraction decreases due to more stable PBL and the enhanced solar heating by smoke particles within and above clouds. However, during night (bottom row), the change of local wind (include sea breeze) induced by the feedback of smoke lead to a more convergence over Karimata strait and south coastal area of Kalimantan during the night time, hence cloud fraction increases denotes increase, and denotes decrease. See the text in Sect. 6 for details.